Plant Physiology®

Plant Physiology, 2024, 00, 1–20
https://doi.org/10.1093/plphys/kiae237
Advance access publication 3 May 2024
Research Article

Development of a mobile, high-throughput, and low-cost image-based plant growth phenotyping system

Li'ang Yu,[†] Hayley Sussman,[†] Olga Khmelnitsky, Maryam Rahmati Ishka, Aparna Srinivasan, Andrew D.L. Nelson,[*] and Magdalena M. Julkowska[*]

The Boyce Thompson Institute, Ithaca, NY 14850, USA
[*]Author for correspondence: an425@cornell.edu (A.D.L.N.), mmj55@cornell.edu (M.M.J.)
[†]These authors contributed equally to this work.
The author responsible for distribution of materials integral to the findings presented in this article in accordance with the policy described in the Instructions for Authors (https://academic.oup.com/plphys/pages/General-Instructions) is Magdalena Julkowska (mmj55@cornell.edu).

Abstract

Nondestructive plant phenotyping forms a key technique for unraveling molecular processes underlying plant development and response to the environment. While the emergence of high-throughput phenotyping facilities can further our understanding of plant development and stress responses, their high costs greatly hinder scientific progress. To democratize high-throughput plant phenotyping, we developed sets of low-cost image- and weight-based devices to monitor plant shoot growth and evapotranspiration. We paired these devices to a suite of computational pipelines for integrated and straightforward data analysis. The developed tools were validated for their suitability for large genetic screens by evaluating a cowpea (*Vigna unguiculata*) diversity panel for responses to drought stress. The observed natural variation was used as an input for a genome-wide association study, from which we identified nine genetic loci that might contribute to cowpea drought resilience during early vegetative development. The homologs of the candidate genes were identified in Arabidopsis (*Arabidopsis thaliana*) and subsequently evaluated for their involvement in drought stress by using available T-DNA insertion mutant lines. These results demonstrate the varied applicability of this low-cost phenotyping system. In the future, we foresee these setups facilitating the identification of genetic components of growth, plant architecture, and stress tolerance across a wide variety of plant species.

Introduction

Plant phenotyping provides a critical layer of information that helps to decipher biological processes and genetic mechanisms related to plant growth and development in response to various environmental factors (Fahlgren et al. 2015a, 2015b; Tardieu et al. 2017; Zhao et al. 2019). Plant phenotypes can differ in spatial and temporal resolution, and reflect plant biochemistry, physiology, morphology, as well as agronomic performance. High-throughput plant phenotyping aids fundamental biology research and plant breeders alike through the identification and enhancement of traits related to disease resistance, plant performance, and environmental resilience. Traditionally, plant phenotypes were collected using manual and destructive methods, associated with high experimental cost, limited throughput, and inconsistencies in data based on subjective interpretation of the observations (Furbank and Tester 2011; Walter et al. 2015). Over the last two decades, image-based technologies and the integration of robotics resulted in a more widespread adaptation of diverse approaches to nondestructively capture plant growth, architecture, and physiology (Fiorani and Schurr 2013; Yang et al. 2013). These nondestructive methods have propelled plant science research forward by allowing for a higher number of replicates, standardization of measurements, as well as increased spatial and temporal resolution. The increased throughput of an experiment allows for screening large populations of plants which can be further utilized in forward genetic screens (Chawade et al. 2019), or study the effect of various biostimulants (Rouphael and Colla 2020). However, many phenotyping solutions still require substantial monetary investment, or extensive engineering experience, which is not widely accessible at the lab, department, or even university/institute level.

The surge in availability of low-cost computers and microcontrollers, such as Raspberry Pi and Arduino, has resulted in the development of cost-effective phenotyping platforms, leading to greater flexibility and affordability of plant phenotyping (Ellison Mathe et al. 2022; Kondaveeti et al. 2022). Some of the previously developed systems can be utilized to capture seed germination, shoot, and root (Dhondt et al. 2014; Czedik-Eysenberg et al. 2018; Colmer et al. 2020; Feldman et al. 2021; Bethge et al. 2023; Li et al. 2023; Ohlsson et al. 2024). Most of the developed applications such as PhenoTiki or PYM rely on top-view imaging (Minervini et al. 2017; Valle et al. 2017), which is suitable in plants growing in horizontal plane or field conditions with unlimited vertical space to accommodate sufficient plant-camera distance. The PhenoBox setup (Czedik-Eysenberg et al. 2018) utilizes the side-view imaging of plants with complex architecture. However, its high costs can be prohibitive for many laboratories to adopt. While these low-cost solutions diversify image-based phenotyping, they require extensive engineering experience and equipment, as well as proficiency in programming and data analysis. Hence, there is an increasing demand for cost-effective phenotyping solutions that offer both low-cost hardware and streamlined data analysis approaches accompanied by clear instructions for ease of use, catering to a wider scope of users. The

Received January 8, 2024. Accepted April 10, 2024.

high-throughput nature of image-based phenotyping is driven by image-processing software (Berry et al. 2018; Das Choudhury et al. 2019; Jiang and Li 2020). The development of plant computer vision (PlantCV) was an important milestone for plant phenotyping, offering a high level of flexibility within image processing pipelines using custom Python scripts (Fahlgren et al. 2015a). The open-source nature of PlantCV and its high volume of users resulted in further extensions to wider applications, and community contributions, and ensured the sustainability of the software (Gehan et al. 2017; Berry et al. 2018; Hodge et al. 2021; Alberto Gutierrez Ortega et al. 2021; Casto et al. 2022). While PlantCV offers pipelines to analyze images being produced by RGB (Red–Green–Blue), hyperspectral, and chlorophyll fluorescence camera scripts (Fahlgren et al. 2015a), RGB cameras remain the most widely accessible and thus have the highest application for plant research. Based on RGB images, traits such as plant area, convex hull, width, and height can be evaluated automatically, once the pixels belonging to the plant are isolated from the background (Gehan et al. 2017). Phenotypes related to tissue color and disease symptoms can be extracted after parametrization of the pipeline or training with machine learning modules (Abbasi and Fahlgren 2016). Plant architecture traits, such as the number of branches, can also be extracted, however, the precision of the automated trait extraction is highly dependent on plant species and complexity (Godin 2000). PlantCV has successfully been adopted for the evaluation of a growing number of crops, including maize (*Zea mays*), rice (*Oryza sativa*), cassava (*Manihot esculenta*), and more (Hairmansis et al. 2014; Kolhar and Jagtap 2023). While the available image-processing tools form a robust basis of image-based phenotyping (Rossi et al. 2022; Zhang et al. 2022), most of them are characterized by a strong reliance on computational user expertise. Computational pipelines often require either generating customized scripts for large-scale data processing or producing self-trained parameters for machine learning purposes. Additionally, adapting imaging hardware and software from diverse sources requires extensive optimization by end users. The programming and engineering requirement for plant phenotyping forms a substantial hindrance in the widespread application of low-cost phenotyping solutions. Thus, a low-cost phenotyping solution with integrated hardware and software, as well as the ability to accommodate a wide range of plants, is sorely needed.

Research into environmental stress resilience, particularly concerning freshwater availability, is crucial for safeguarding future agricultural productivity. Drought impacts 80% of farmlands worldwide, and this percentage is growing with the progressing climate change (Meza et al. 2020). Reduced rainfall and shrinking water supplies in the soil lead to reduced crop growth, transpiration, and yield, resulting in an agricultural drought (Satoh et al. 2022). Prolonged periods of reduced water supply lead to gradual depletion of soil water supplies, taking place over months or years, resulting in hydrological drought (Satoh et al. 2022), which forces agricultural systems to adapt to this new reality. Plants evolved several mechanisms to adapt to drought stress conditions, including signaling pathways to limit water loss through transpiration (Hughes et al. 2017) synthesis of compatible solutes that serve as osmolytes to help with turgor maintenance, efficient water extractions, and protection from oxidative damage (Akashi et al. 2001). Partitioning biomass into steep, cheap, and deep root systems can enhance scavenging for deeper layers of water resources (Grieder et al. 2014), whereas maintenance of a large root/shoot ratio prioritizing water acquisition over (Chen et al. 2004). While most drought research has thus far been performed in staple crops and Arabidopsis, the indigenous crops used by smallholder farmers are becoming prominent objects of interest for more insight into drought resilience (Cullis and Kunert 2017). The application of drought stress varies tremendously across scientific literature, ranging from complete water withdrawal (Choudhury et al. 2022) to exposing the plants to osmotic agents, such as mannitol, sorbitol, or polyethylene glycol (Trontin et al. 2014). Various applications of drought stress highlight the specific aspects of drought stress responses selected by the researchers, each with its own advantages and drawbacks (Harrison et al. 2014). While soil-based water withdrawal experiments are prevalent due to relatively low effort requirements, these setups do not account for variable water-use by the plants, and typically favor genotypes that restrict their transpiration, and thus are able to conserve the water more efficiently (Correa et al. 2019). On the other hand, watering the plants to lower soil water-holding capacity is accounting for differences in transpiration, but requires time-consuming daily watering to the reference weight of each pot. Maintenance of lower soil water-holding capacity mimics mild drought stress, which occurs most frequently, based on the historical records (Harrison et al. 2014). Image-based phenotyping approaches have been applied to monitor plant growth under water scarcity (Petrozza et al. 2014; Correa et al. 2019; Marchetti et al. 2019), however, the availability of image-based tools is restricting the number of species that have been studied thus far. Hence, there is a growing need for protocols and experimental setups suitable for high-throughput plant phenotyping are necessary.

The above arguments motivated the development of an open-source system consisting of three hardware setups (PhenoRig, PhenoCage, and AWWESmo) and easy-to-use computational pipelines that streamline image collection, watering individual pots to their respective target weight, and data analysis. Our system was built using low-cost and lightweight materials, which can be used to effectively monitor physiological responses in response to stress across a wide variety of species. This integrated system substantially reduces the cost and time necessary to collect reproducible image and evapotranspiration data and lowers the computational barrier to extract phenotypic data (RaspiPheno Pipe). Moreover, the developed shiny app (RaspiPheno App) is a dynamic tool for downstream statistical data analysis, sample comparison, and data interpretation. To demonstrate the system's capacity, we used the developed tools to screen a natural diversity panel of 368 cowpea genotypes and, through the Genome-Wide Association Study (GWAS), identified genes associated with drought response during early vegetative growth. The described suite of phenotyping solutions, as well as data analysis pipelines, will promote affordable plant phenotyping and accelerate the discovery of genes and physiological traits contributing to stress resilience.

Results

Phenotypic hardware design of the system

To increase the accessibility of plant phenotyping, we developed a set of mobile, affordable, and customizable phenotyping setups. The setups were designed to fit into conventional growth chambers with limited vertical space (Fig. 1) and allow the evaluation of plants with different types of architecture. The top-view PhenoRig setup was designed to image the growth of plants for which the majority of growth occurs within two dimensions, such as Arabidopsis rosettes (Fig. 1A). Plants with more complex architecture can be imaged using side-view PhenoCage setup

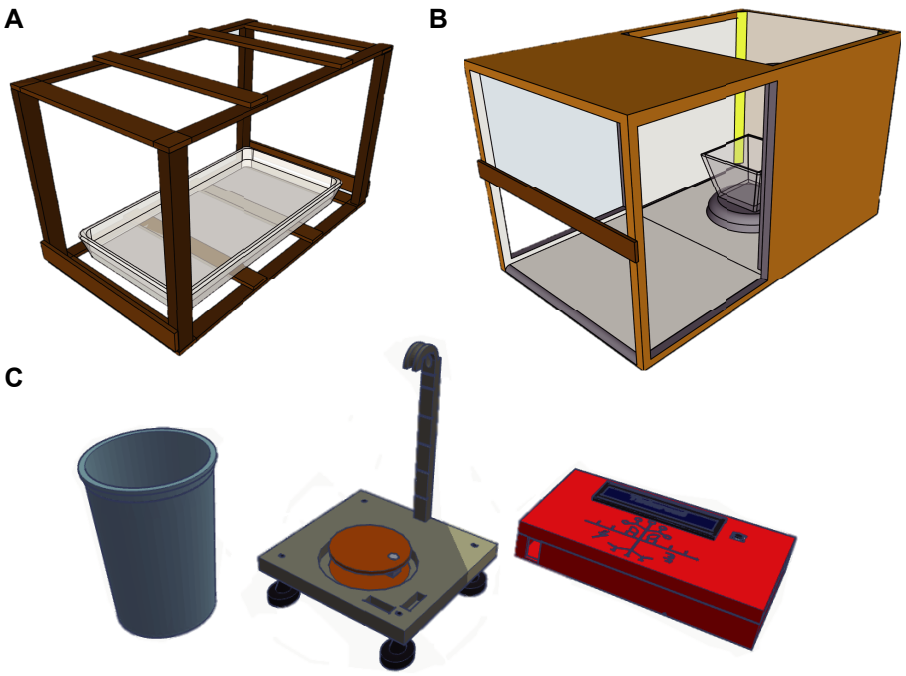

Figure 1. PhenoRig, PhenoCage, and AWWEsmo: three facilities were constructed using lightweight materials with 3D printed accessories for data collection purpose. **A)** PhenoRig system: including a frame to hold two Raspi cameras and a Raspi computer. A tray holding plants is placed at the bottom of the frame to display plants' top-view characteristics. **B)** PhenoCage system: including a frame to hold one Raspi camera and a Raspi computer. A rotating booth is placed at the center of the cage with a constant rotation rate to represent plant architectures from different sides. **C)** AWWESmo system: including a container for water replenishment (blue), and a water pump that integrates a weight scale controlled by an Arduino Uno R3-derived console (red). Precise water replenishment is executed by the input weight (grams) of the console.

(Fig. 1B). Within PhenoCage setup a plant is positioned on a rotating platform, and seven consecutive images are taken to adequately capture the projected shoot area as the estimation of plant's digital biomass. To monitor plant evapotranspiration, we developed an Automatic Weighing and Watering device to study Evapotranspiration (AWWEsmo) that automatically records pot weight and waters it to the reference weight (Fig. 1C). AWWEsmo accuracy relies on a HX711 load cell, which was reported to drift across varying temperatures, and thus requires frequent calibration. While the platforms we developed here consist of low-cost materials that have limited lifespan and accuracy, the individual components could be replaced by higher quality components driven by more advanced sensor technologies for increased precision. Within the experimental conditions described below, we did not experience low accuracy of AWWEsmo, as compared to the 0.1 g laboratory scale (Supplementary Fig. S1). However, we did observe reduced accuracy when the device was used in growth chambers with substantially different temperature (Supplementary Fig. S1), and thus advice for the developed AWWEsmo device to be calibrated within the growth chamber conditions and checked frequently for its accuracy.

The individual devices rely on Raspberry Pi computers (PhenoRig and PhenoCage) and Arduino microcontrollers (AWWEsmo) for data acquisition, which lend themselves to flexible and cost-effective setups that can be easily adapted to accommodate a wider range of species or alternative hardware components. The PhenoCage can be used to monitor the growth of Arabidopsis continuously, using an automatically deployed imaging command, while PhenoRig and AWWEsmo require the user to feed the plants into the setup and deploy the image/measure command manually. The current design of PhenoRig allows imaging of a standard full tray of Arabidopsis plants with two cameras, where each camera can capture a grid of 4×4 plants (Fig. 2A), with the total capacity of PhenoRig being an 8×4 plant grid. PhenoCage, on the other hand, has a capacity of one plant, as the complex 3D architecture of the shoot does not permit simultaneous imaging of multiple plants. To ensure the best results in image processing, we recommend putting two to four white tags on top of the pots for PhenoRig, to correct for white balance between the individual images, and calibrate the projected shoot size into mm^2 (Fig. 2B). For the PhenoCage, we suggest using a white background for white balance corrections (Fig. 2, A and B). As the distance between the plant and camera in the PhenoCage setup is determined per plant species, and the sum of projected pixels from seven side view angles will be larger than the shoot projected area, thus we do not recommend recalculating the projected plant size from pixels into projected leaf area (mm^2), but rather keep it in artificial units (pixels). Additional accessories installed for image collection and illumination, include RasPi cameras, LED lights, LCD touch screens, and 3D-printed accessories holders (Supplementary Figs. S2 and S3).

To effectively address data analysis of images collected over multiple days and devices, we developed a computational pipeline (RaspiPheno Pipe) that automates image distribution, storage, and subsequent data extraction based on experimental design into a repeatable workflow (Fig. 3). This pipeline parallelizes image segmentation steps and deploys them on batches of images to examine projected shoot area and architectural traits (Fig. 3). This optimized image extraction process requires (1) the positional information of white balance markers and region of interest (ROI, Fig. 2), (2) specific thresholds and coordinates used for extracting plant objects from RGB images, and (3) storage locations for input and output files. Quantitative data generated and organized by the RaspiPheno Pipe can be analyzed using the RaspiPheno App,

Figure 2. PhenoRig and PhenoCage images. **A)** RGB images output of Raspi camera of Arabidopsis (left panel) and tepary bean (right panel). The red squares highlight the area used for white balance correction in the subsequent steps. Blue squares indicate the ROIs for image processing. **B)** Output images after processing using PlantCV pipeline. The blue edge highlights the perimeter of the leaf area (green tissue) and the purple edge defines the convex hull area of each individual plant.

an interactive and programming-free analytical application powered by the Shiny R package (https://rstudio.github.io/shiny/authors.html). RaspiPheno App was designed to address the statistical analysis of data associated with shoot area and architectural traits among customized independent variable groups (e.g. genotypes or treatments). Within RaspiPhe App the user can match the information on genotype and treatment with quantitative values from each plant as the data reshaping process (Fig. 3). The integrated data are then presented as time-series graphs, and user can perform data curation to smooth noisy data and generate a predicted, or transformed dataset (see Methods). Alternatively, the user can generate a clean dataset by removing data points beyond the standard deviation (SDS) of values predicted by the smoothing function. RaspiPheno App can calculate the growth rate for the user within a customized time interval (e.g. 12 or 24 h) to characterize the differences in plant growth under different conditions using pairwise or multiple-group tests (Fig. 3). More information on using RaspiPheno App can be found at (https://github.com/Leon-Yu0320/BTI-Plant-phenotyping/tree/main/RasPiPheno_APP).

Together, the RaspiPheno Pipe and RaspiPheno App provide an integrated framework for extracting data from images and quickly analyzing the phenotypic data. As a web-browser integrated RShiny application, the RaspiPheno App streamlines what is typically a command line-based statistical analysis into an intuitive and interactive process. As the developed tools have limited computational requirements, they can be run on a standard laptop with an internet connection. We aim for these open-source hardware and software packages to simplify the data extraction process that often hinders data analysis and delays scientific progress.

The instructions for constructing system hardware using inexpensive wooden or aluminum frames can be accessed at protocols.io (Yu and Julkowska 2022), whereas the necessary parts for constructing each setup are listed in Supplementary Tables S1 to S3. The RaspiPheno App and RaspiPheno Pipe are available, along with the detailed instructive user manuals and example datasets, on the GitHub repository (https://github.com/Leon-Yu0320/BTI-Plant-phenotyping). Together, PhenoRig, PhenoCage, and AWWEsmo represent a basic suite of plant phenotyping tools that significantly accelerate research and can be instrumental in screening populations of accessions or mutants under diverse conditions. The construction of each setup requires minimal financial investment (less than 200 USD) and thus contributes to democratizing plant phenotyping tools in a wide range of potential users.

Stress-induced changes in Arabidopsis, cowpea, and tepary beans

To test the efficacy of the developed tools, we evaluated the images produced by our setup for their sensitivity to detect the effect of abiotic stress on three species—Arabidopsis, cowpea, and tepary beans (Figs. 4 and 5). Arabidopsis Col-0 plants were treated with salt stress (100 mM NaCl effective concentration) 2 wk after germination and imaged every 30 min for the following 2 wk. This method has been previously described in (Awlia et al. 2016), and applied to the Arabidopsis diversity panel, without any

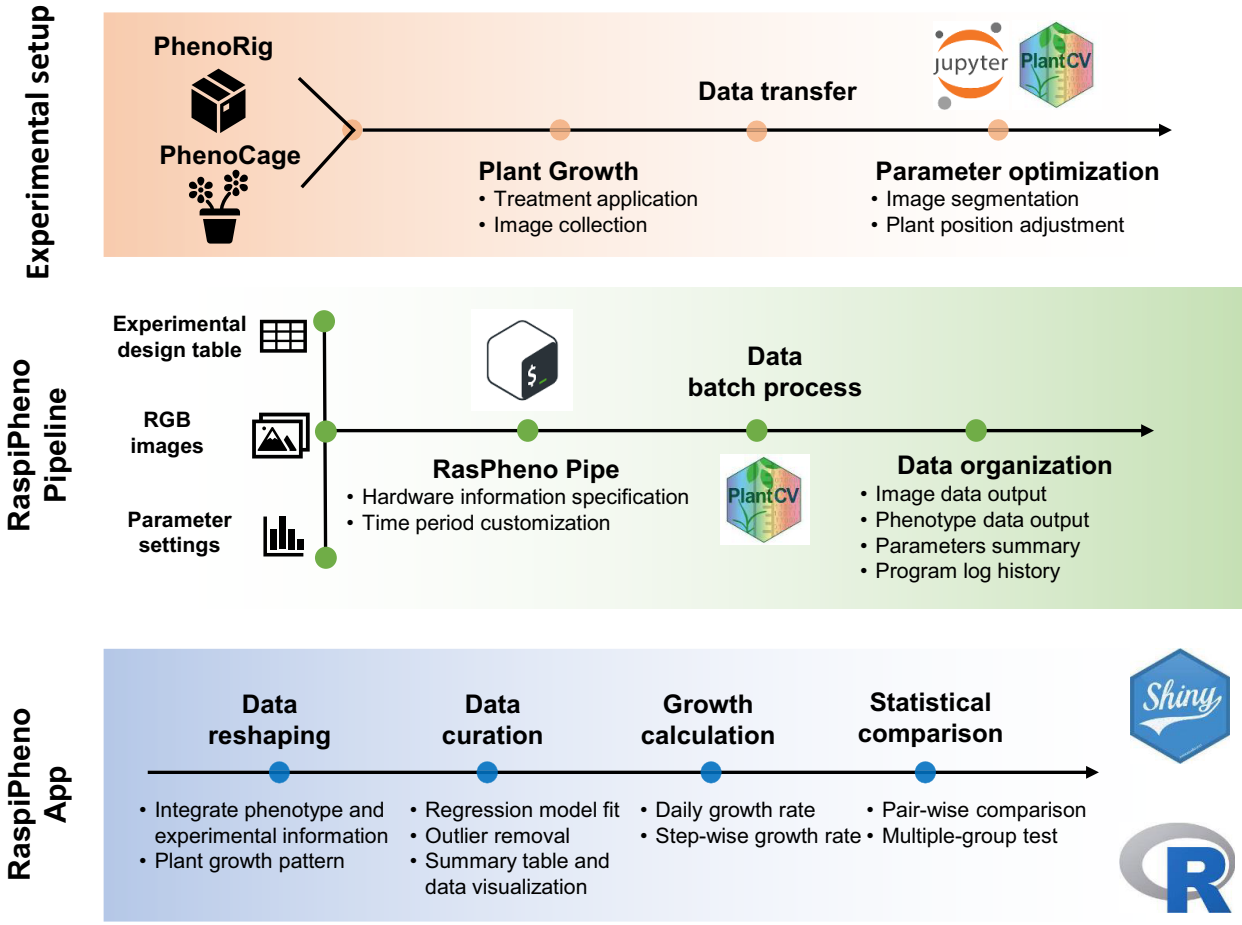

Figure 3. Overview of the Pheno-Computational pipeline. The experimental setup consisting of PhenoRig (Arabidopsis) or PhenoCage (larger plants with 3D architecture is used to collect data on plant growth and architecture). Using the first few images obtained by the experimental setup system, the image acquisition parameters are optimized for best image processing in the subsequent steps. The phenotypic data processing is based on PlantCV pipeline integrated into RaspiPheno Pipe, which applies batch-specific parameters (*parameter settings table*) onto a batch of *RGB images* (indicated in the *experimental design table*) to perform batch-specific processing. Subsequently, the quantitative data from RaspiPheno Pipe can be uploaded along with the metadata, containing genotype and treatment information for individual plants, into RasPiPheno App, where the data is matched, curated, processed for outliers and custom calculations of plant growth rate and statistical comparisons are performed.

observation of premature leaf senescence (Awlia et al. 2021). We observed a consistent decrease in rosette size starting from 6 d after induction of salt stress (Fig. 4A). While continuous imaging can provide highly detailed information, it is also prone to variation due to leaf movement throughout the day. To reduce this variation, the rosette size data was modeled over the entire experimental time course using a smooth spline function within PhenoApp (Fig. 4B). Smooth spline modeling provides the means for smoothing noisy data through function estimates, balancing a measure of goodness of fit with a derivative based measure of the smoothness. Moreover, smooth spline functions can be deployed to identify potential outliers and eliminate specific points from the data set based on standard deviations from the spline (Fig. 4C). Plotting the increase in the rosette size of individual plants using smooth splines significantly reduced the noise caused by diurnal movements of leaves, and thus provides a clearer image of the plant's growth trajectory. We used the collected data to calculate daily rosette growth rate by fitting a linear regression to daily changes in rosette size, and plotting the change in growth rate throughout the experiment. The daily growth rate decreased significantly within 2 d of salt treatment application (Fig. 4D). The difference in growth rate between control and salt-stressed plants increased over the duration of the experiment (Fig. 4D). These results suggest that our PhenoRig setup allows us to identify differences between plants grown under control and salt stress conditions with high sensitivity, detecting significant differences as early as 2 d after stress in daily rosette growth rate.

To evaluate the efficacy of the PhenoCage setup for more complex plant architectures, five cowpea accessions and two tepary accessions were exposed to drought stress at 17 d after germination. For the two weeks after stress application, the weight of each pot was monitored and adjusted by replenishing freshwater daily using AWWEsmo, while changes in shoot size were recorded every 2 d using the PhenoCage setup (Fig. 5). We did not account for increased plant size throughout the experiment, and the target weight was determined for each pot based on the soil weight alone. As some plants required additional support structure, due to their climbing or prostrate growth habit, we designed a stackable 3D printed trellis, which resulted in minimal obstruction of the imaged plant area (Supplementary Fig. S4). Drought stress was applied through a gradual reduction in soil water-holding capacity from 60% to 10% for both cowpea and tepary beans. The differences between control and drought stress plants were observed after 5 and 6 d for cowpea and tepary beans, respectively (Fig. 5, A and B). We observed a high correlation

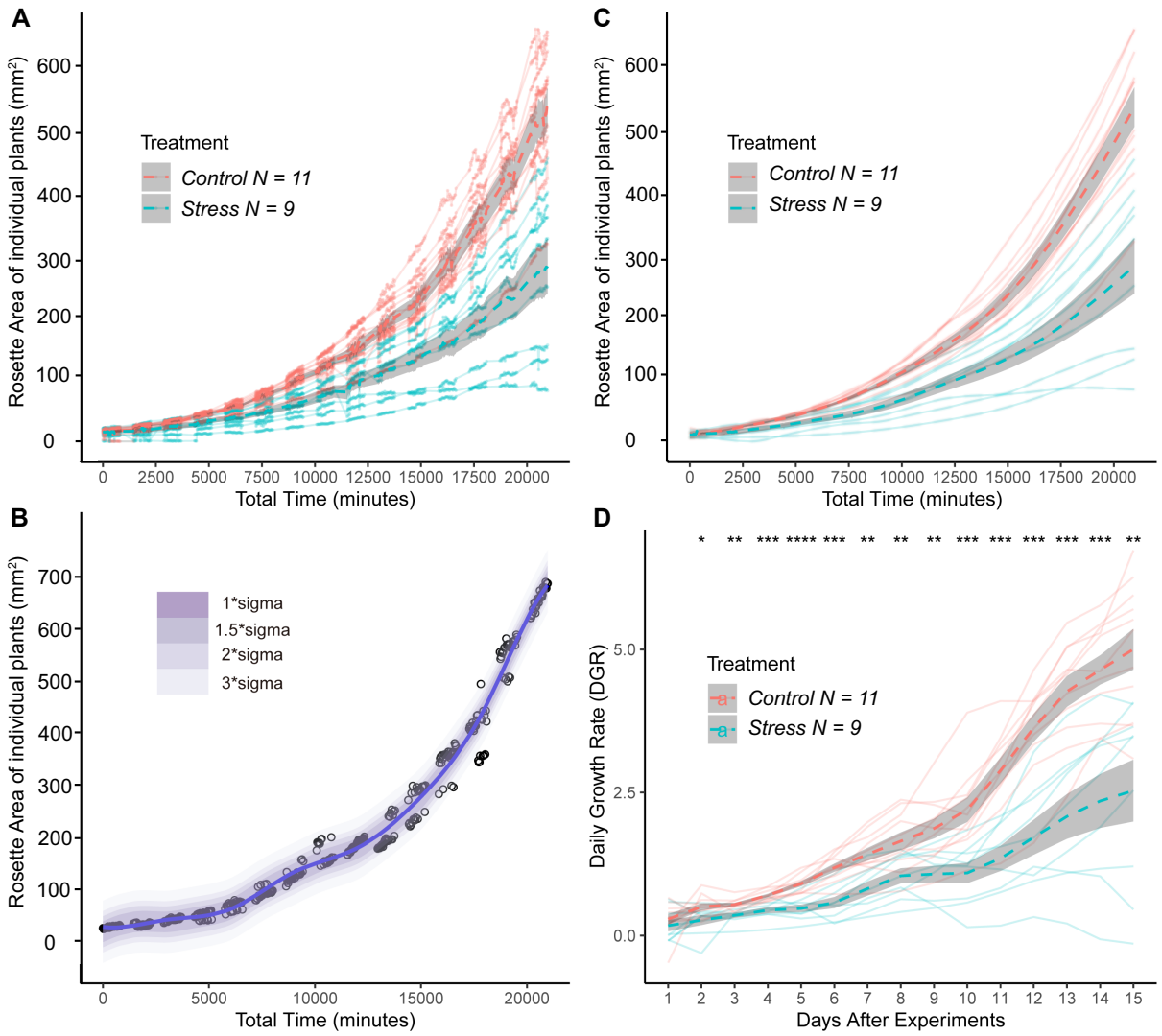

Figure 4. Example of Arabidopsis PhenoRig data. Arabidopsis seedlings were exposed to salt stress 2 wk after germination. The trays containing Col-0 seedlings exposed to salt stress/mock treatment (Control) were placed under PhenoRig setup and imaged every 30 min for 2 wk. **A)** The increase in the projected rosette area was observed over 2 wk following the salt stress exposure. Each solid point represents one data point, along with mean values (dashed lines) and standard error (gray shaded area) represented (applies to panels C and D). **B)** In order to reduce the noise in data, we curated data for each individual plant using smooth spline function with different levels of sigma to identify data points as potential outliers. **C)** Data derived from the smooth spline function was calculated for all the samples used for imaging within our experiment, which significantly reduced noise levels. **D)** The smooth spline data was subsequently used for calculating the daily growth rate for each measured plant. The difference in daily growth rate between plants exposed to control and salt stress treatment was calculated using a *t*-test. The *, **, ***, and **** represent *P*-values below 0.05, 0.01, 0.001, and 0.0001, respectively.

($R = 0.92$ for cowpea and $R = 0.95$ for tepary) between the plant fresh weight and projected shoot area recorded on the final day of the experiment for both cowpea and tepary beans (Fig. 5, C and D), indicating the high reliability of the PhenoCage system to nondestructively estimate the changes in digital biomass. When we calculated the growth rate for each plant throughout the entire experiment, we observed significant differences between genotypes and treatments for tepary bean and cowpea alike (Fig. 5, E and F). The weight of the pot and watering data, collected through AWWEsmo, was used to calculate the daily evapotranspiration rate for each plant. As the target drought weight was reached 2 d after the initial treatment application, the differences in evapotranspiration were also evident within 2 d after monitoring soil water-holding capacity (Supplementary Fig. S5). Evapotranspiration of tepary beans and cowpeas substantially decreased in response to drought stress (Fig. 5, G and H). High variability of growth rate and evapotranspiration of cultivated tepary beans (reflected by high standard deviation) corresponded to the high variation in plant size exhibited by this genotype within the experiment (Fig. 5, F and H). When comparing the median evapotranspiration per plant throughout the entire experiment (Fig. 5, G and H), significant differences were observed exclusively under drought stress conditions. Cowpea accessions Suvita-2 and UCR779 showed the highest and lowest evapotranspiration under drought stress, respectively. Cultivated tepary bean accession (TDP-22) showed higher rate of evapotranspiration compared to the wild tepary bean accession (TDP-359). We did not calibrate the evapotranspiration results to daily transpiration rates due to high trait complexity, as the substantial portion of evapotranspiration constitutes water evaporation from the pot. Nevertheless, AWWEsmo allowed us to impose reproducible drought stress conditions for all studied plants. The above results indicate that

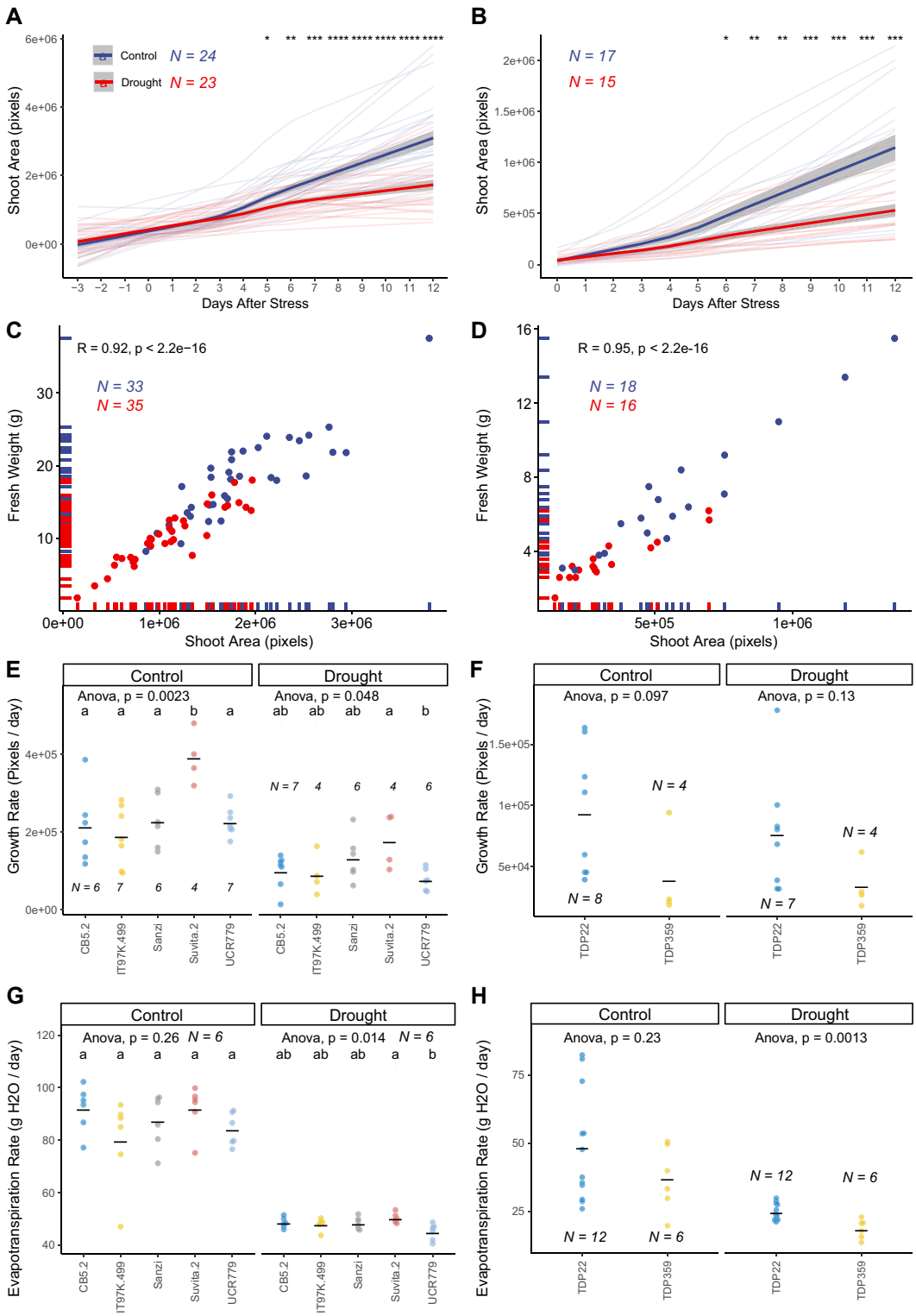

Figure 5. Examples of cowpea and tepary bean data were collected using PhenoCage and AWWEsmo setups. The seedlings of five cowpea accessions and two tepary bean accessions were germinated for 17 d, and exposed to control treatment or drought stress (60% and 10% soil water-holding capacity, respectively). **A)** The increase in shoot area was modeled using the smooth spline function over the recorded data for cowpea with mean values represented by bold lines and the standard error by shaded area. **B)** Tepary bean over the course of 12 d following the drought stress application (average values and standard error were visualized by bold lines and gray shaded area). The difference between treatments was calculated using ANOVA with *, **, ***, and **** indicating the *P*-values below 0.05, 0.01, 0.001, and 0.0001, respectively. The Pearson correlation between the projected shoot area and the fresh weight of the shoot recorded at the last day of the experiment was examined in both (**C**) cowpea and (**D**) tepary bean. The growth rate was calculated based on the smooth spline modelled data for (**E**) five cowpea accessions and (**F**) two tepary bean accessions for individual conditions. The median evapotranspiration rate, was calculated based on the data collected using AWWEsmo for (**G**) five cowpea accessions and (**H**) two tepary bean accessions. The mean values per group were marked by black horizontal lines and the effect of the genotype within individual treatment was tested using ANOVA, and the significantly different groups of cowpea accessions were additionally determined using Tukey HSD test (*P*-value < 0.05).

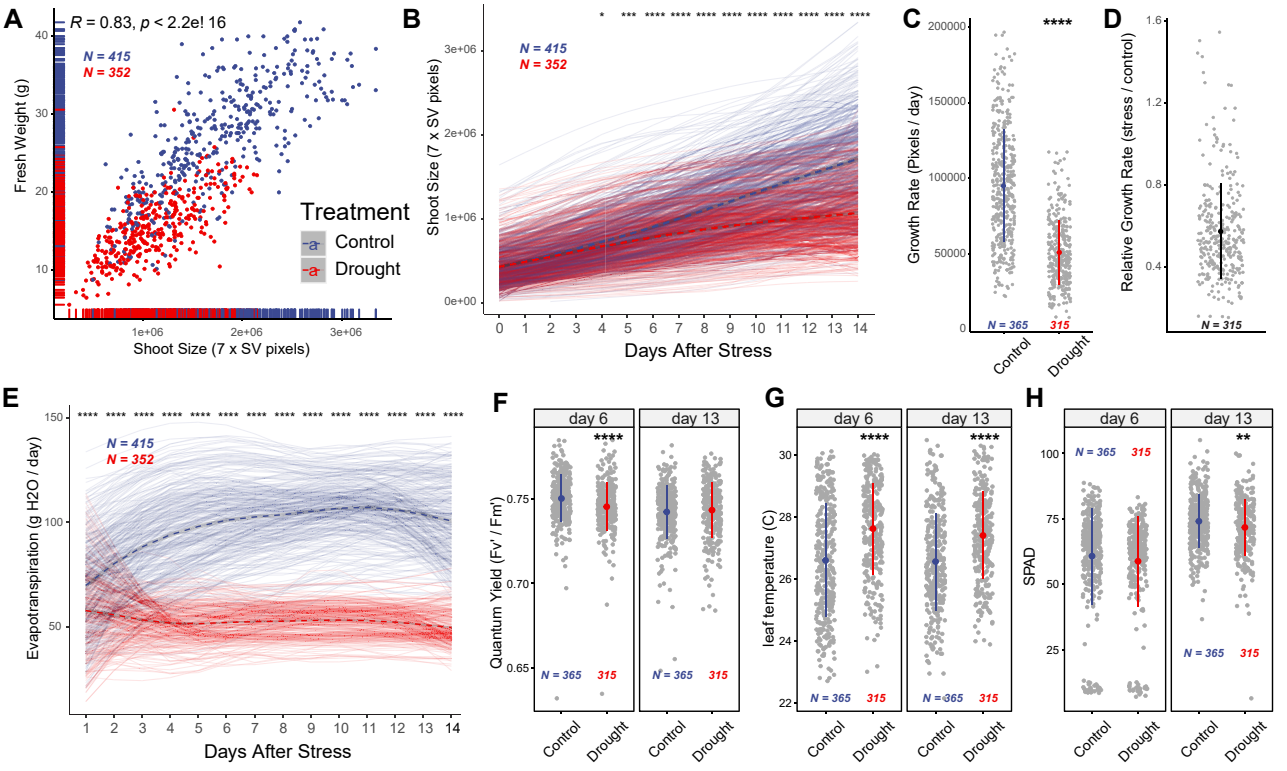

Figure 6. Drought stress-induced changes in natural diversity panel of cowpea. Three hundred and sixty-eight accessions were exposed to 20% soil water-holding capacity (SWHC—Drought) or 60% (SWHC—Control) 16 d after sowing. The plants were monitored for an increase in shoot biomass and evapotranspiration over the period of 2 wk. **A)** Correlation between digital biomass and fresh weight on the last day of measurement. Pearson correlation coefficient (*R*) and *P*-value of the correlation are presented in the upper left corner of the graph. **B)** Increase in digital biomass over the experiment for plants exposed to control and drought treatments: Each solid line represents data for each sample, with dashed lines standing for mean value and gray shaded area for standard error (SE), **C**) The growth rate was calculated by fitting linear function to digital biomass for each accession for the duration of the treatment with gray dots stand for each sample and the colored dots for mean value (applies to panels **D**, **F**, **G**, and **H**). **D**) Relative growth rate was calculated for each accession by dividing the genotype-specific growth rate recorded under drought conditions by the growth rate recorded under control conditions. **E)** Evapotranspiration was estimated for each plant by measuring the pot weight every day of the experiment, watering it to the reference weight, and calculating the difference in weight between consecutive days (solid lines and gray shaded area correspond to mean value and standard error). The (**F**) quantum yield (F_v'/F_m'), (**G**) leaf temperature (**C**) and (**H**) chlorophyll content were measured using the PhotoSynQ MultiSpeq device. The significant differences between control and drought stress were tested using a Student's *t*-test, and *, **, ***, and **** represent *P*-value < 0.05, 0.01, 0.001 and 0.0001, respectively.

PhenoCage and AWWEsmo can detect differences between treatments as well as subtle differences in plant growth rate and evapotranspiration between genotypes for plants with complex architecture, such as cowpea and tepary beans.

Drought-stress-induced changes in the cowpea diversity panel

To illustrate the suitability of the developed system for a capacity required by a high-throughput phenotyping experiment, we screened a cowpea miniCore diversity panel (Muñoz-Amatriaín et al. 2021), consisting of 368 accessions, for drought stress-induced changes in growth rate, evapotranspiration, and photosynthetic efficiency (Supplementary Tables S4 and S5). One replicate per accession per treatment was germinated in well-watered conditions. Once 80% of the plants developed the first trifoliate leaf, pot weight was monitored and adjusted to target weights, corresponding to 60% and 20% of soil water-holding capacity for control and drought stress, respectively. Daily evapotranspiration was monitored for 14 d, with digital plant biomass collected every other day with the PhenoCage. Additional measurements on photosystem II efficiency were collected from each plant at 6 and 13 d after stress application. At the end of the experiment, fresh weight data were collected from shoot material for each plant.

As in pilot experiments, the high correlation between fresh weight and projected shoot area (Fig. 6A) indicated that our PhenoCage system produces a good estimate for digital plant biomass. Tracking progression in shoot size allowed shoot growth to be modeled using smooth splines, revealing significant differences in shoot size starting from 4 d after initial drought stress application (Fig. 6B). Based on the increase in shoot area, the growth rate was also estimated for each genotype, with significant differences observed between control and drought stress conditions (Fig. 6C, Supplementary Table S6). Additionally, the relative impact of stress on growth rate was calculated for each genotype by dividing the genotypic mean growth rate observed under drought stress conditions by the genotypic mean growth rate observed under control conditions (Fig. 6D, Supplementary Table S6). While on average, growth rate was reduced to 0.6 of the rate observed under control conditions, 19 accessions displayed increased vigor under drought stress (relative growth rate > 1, Supplementary Table S6), while 64 accessions showed severe drought stress sensitivity (defined as relative growth rate < 0.4, Supplementary Table S6). Upon further inspection, we identified that most of the high-vigor accessions showed relatively small postures and slow growth rate under control conditions. As the data presented here is based only on one experimental replicate, the validation of the accessions showing low and high vigor is necessary using more biological

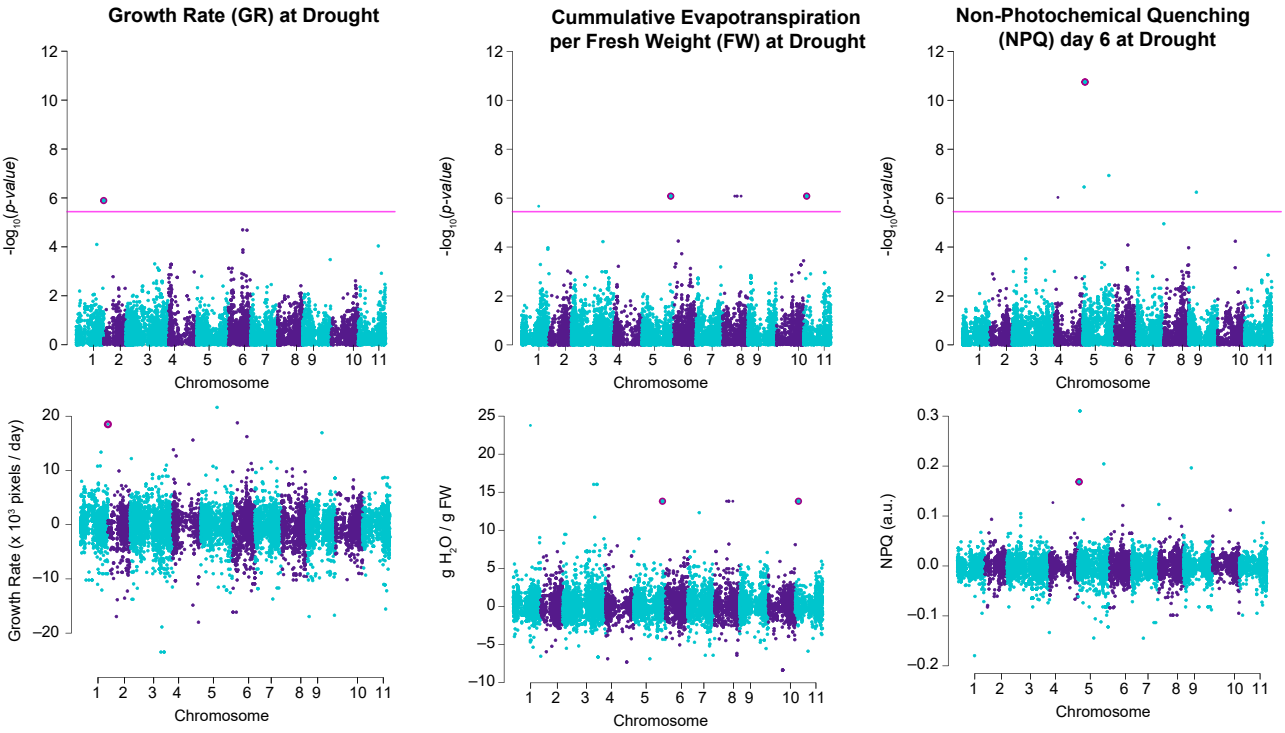

Figure 7. Identification of genetic components of drought stress responses in cowpea through GWAS. GWAS was performed using ASReml-based script on 368 accessions using 42,711 SNPs and kinship matrix as a co-factor. GWAS associations were examined for overlap between control and drought stress conditions, −log10(*P*-value) score, minor allele frequency, and effect size. The selected associations that were observed exclusively for drought stress-treated plants are highlighted in pink. The upper panel represents Manhattan plots, with a pink line representing the Bonferroni threshold (equal to −log10(0.05/# SNPs). The bottom panel represents the effect size observed for SNPs. The SNPs selected for further investigation (**Supplementary Table S9**) are highlighted with dark-pink outline.

and experimental replications. Drought-treated plants transpired significantly less water than control plants (Fig. 6E), and on average, the evapotranspiration decreased to 0.55 of the levels observed under control conditions (Supplementary Fig. S6, Supplementary Table S7). While drought stress was observed to reduce quantum yield (F_v'/F_m') only during the early phase of the experiment (Fig. 6F, Supplementary Table S7), a decrease in chlorophyll content (SPAD) was observed only at the later stage of the experiment (Fig. 6H, Supplementary Table S7). On the other hand, the drought stress significantly increased leaf temperature both at the early and late stages of drought stress treatment (Fig. 6G). In summary, these results illustrate that variability in drought stress responses across a large and diverse panel of plants with complex architecture can be captured through our PhenoCage setup.

Identification of genes underlying drought responses

To identify genetic components underlying the diversity observed in the cowpea miniCore population (Fig. 7), we used the collected phenotypic data in combination with the SNPs acquired from SNP array (Muñoz-Amatriaín et al. 2021) as input for a GWAS (Supplementary Table SS7). We examined the identified associations for their association strength and predicted effect size (Fig. 7). In total, we identified 59 significantly associated SNPs, which could be grouped into 25 loci, based on SNPs falling into 30 kb window (corresponding to genome-average linkage disequilibrium within cowpea genome, Supplementary Table S8). In total, we identified 10 loci specific to control conditions, 12 drought-specific loci, and 3 loci shared between the traits measured under control and drought stress conditions (Supplementary Tables S8 and S9). Based on the association strength (−log(*P*-value) > 5.45), effect size (ß > 3× SD), and the traits, we prioritized 9 loci for further investigation. For all identified associations, we examined the predicted genes in the genome annotation within the linkage disequilibrium (30 kbps) of identified SNPs (Lonardi et al. 2019).

Growth rate under drought stress was associated with one SNP on chromosome 1, positioned within the coding region of Vigun01g250400, which, according to the genome annotation, is a putative homolog of the Arabidopsis gene AT4G14180, which encodes a Putative Recombination initiation Defect protein (AtPRD1), required for DNA double-strand break formation during meiosis. The two genes directly up and downstream of the associated SNP (Vigun01g250500 and Vigun01g250600) are hypothesized to encode pentatricopeptide repeat and zinc-finger (C2H2 type) family proteins, respectively. We identified two drought-specific associations with evapotranspiration use efficiency under drought stress (Fig. 7, Supplementary Table S9), located on chromosomes 5 and 8. The association on chromosome 5 was found within Vigun05g246700, which is a putative homolog of Arabidopsis AT3G25830, encoding a monoterpene 1,8-cineole synthase (AtTPS-Cin). The monoterpene 1,8-cineole was previously associated with decreased root growth in *Brassica campestris* (Koitabashi et al. 1997), and AtTPS-Cin is expressed in Arabidopsis roots (Chen et al. 2004). The association on chromosome 8 was found within Vigun08g112100, which encodes a putative cowpea homolog of AT2G40690, a nuclear-encoded NAD-dependent glycerol-3-phosphate dehydrogenase family protein associated with flux of fatty acids in the chloroplast (Singh et al. 2016). The neighboring genes (Vigun08g112000 and Vigun08g112200) encode homologs of sucrose transporter (SUT4,

AT1G09960) and transcription factor (WKRY70, AT3G56400) (Supplementary Table S9).

We found the most significant associations with nonphotochemical quenching (NPQ) under drought. However, the majority of these associations (3 out of 5 loci) were also identified under control conditions (Supplementary Table S7). The most prominent drought-specific association was located on chromosome 4, within Vigun04g051200, which encodes a cowpea homolog of Arabidopsis glutaredoxin family protein, AT5G39865 (Supplementary Table S9). To evaluate the function of identified genes in drought stress response, we examined the available homozygous T-DNA insertion lines of the putative Arabidopsis homologs of the identified cowpea candidate genes (Supplementary Table S9, Supplementary Figs. S7 to S10). The available mutants were grown alongside Col-0 wild-type in the soil pots, and at 2 wk after germination, the pot weight was adjusted to target weight corresponding to 60% and 10% soil water-holding capacity for control and drought treatments respectively. The plants were imaged every 30 min using the PhenoRig system, while their weight was recorded and adjusted every second-day using AWWEsmo. The initial screen revealed that out of 43 T-DNA insertion lines, six and two lines developed significantly larger or smaller rosettes, respectively when compared to Col-0 under drought stress conditions (t-test P-value < 0.05, Supplementary Figs. S7 and S8). Eight and four T-DNA insertion lines showed, respectively, increased or decreased evapotranspiration rates under drought stress compared to Col-0 (Supplementary Fig. S9). Nine and two lines showed increased or decreased leaf temperature, respectively, whereas five lines showed a significant decrease in NPQ (Supplementary Fig. S9). In total, six T-DNA insertion lines showed overlap in the measured phenotypes under drought conditions (EVT2 to 2, EVT3-2, EVT6-2, EVT8, GR4-1 and NPQ6-3 targeting 1,8-cineole synthase, alpha carbonic anhydrase 7, WRKY70, CAAX amino-terminal protease family, xyloglucan endo-transglucosylase/hydrolase 16, and pentatricopeptide repeat protein (PPR), respectively, Supplementary Table S9). As it is possible that other alleles targeting these genes were not detected as significantly different from Col-0 due to a low number of replicates ($n = 4$ per genotype per condition), we performed an additional experiment with an increased number of replicates ($n = 12$) (Figs. 8 to 10).

The 13 selected mutants were grown under control and drought (20% soil–water holding) conditions. Under both control and drought conditions, all 13 of the mutant lines used the same amount of water as the Col-0 plants (Supplementary Fig. S10), including the identified loci initially linked to evapotranspiration (Fig. 8). Significantly larger rosettes were observed in the mutant lines targeting genes encoding 1,8-cineole synthase (AtTPS27, EVT2-2), CAAX amino terminal protease (EVT8), Alpha carbonic anhydrase 7 (AtACA7, EVT3-1, EVT3-2) under drought conditions but not under control conditions (Fig. 8, Supplementary Fig. S11). The mutant line targeting WRKY70 (EVT6-2) had significantly ($P < 0.05$; t-test) larger rosettes under both control and drought conditions (Fig. 8, Supplementary Fig. S11). Under control conditions alone, for the last part of the experiment, we observed significantly larger rosette sizes in EVT6-1, which also targets WRKY70 (Supplementary Figs. S11 and S12). For the CAAX protease and AtACA7, we observed that all T-DNA insertion lines targeting these genes showed a significant increase in rosette size (Fig. 8, D and F). AtACA7 is predominantly expressed in root stele (Brady et al. 2007), and its expression under abiotic stress was not reported in previous studies (Kilian et al. 2007). CAAX protease is expressed in the new leaves (Klepikova et al. 2016), and its expression does not change in response to drought or osmotic stress (Kilian et al. 2007). Only one of the two screened T-DNA insertion lines for TPS27 and WRKY70 showed significant increase in rosette size under drought stress (Fig. 8, B and H, Supplementary Fig. S12). Based on the previous data, WRKY70 is expressed in the senescing leaf petiole (Klepikova et al. 2016), but its expression is unaltered by drought stress in Col-0 (Kilian et al. 2007). On the other hand, TPS27 is known to be expressed in the root stele (Brady et al. 2007) and is increased by exposure to osmotic, salt, and drought stresses (Kilian et al. 2007). These results suggest that the identified candidate genes are potentially involved in drought resilience through the maintenance of vegetative growth under both control and drought stress conditions.

Additionally, we observed larger ($P < 0.05$; t-test) rosette size in drought and control plants in three (NPQ6-2, NPQ6-4, NPQ6-5) of the mutant lines targeting the Arabidopsis homolog to the gene associated with NPQ in cowpea, pentatricopeptide repeat superfamily protein (AtPPR, Fig. 9A, Supplementary Fig. S11). For the NPQ6-1 mutant line, significantly larger rosette sizes were observed only under drought stress conditions (Fig. 9B). Variations of the homologous genes among five cowpea genomes that correspond to the *Arabidopsis* AT3G02490 gene (Muñoz-Amatriaín et al. 2021), the 5′ UTR is the predominant site of sequence variation, containing one insertion–deletion mutation and four SNPs (Fig. 9A). The line targeting 5′ UTR in Arabidopsis gene region (NPQ6-2) showed significant changes in rosette size, suggesting that 5′ UTR is indeed playing an important role in this gene function (Fig. 9B). However, as the mutation induced by T-DNA insertion is different in size and character from INDELS in cowpea pangenome, we cannot make any specific conclusions about the role of these mutations. Only one of the five studied insertion lines did not show significant changes in rosette size (NPQ6-3, Supplementary Fig. S12). As the location of this insertion line is beyond the 3′ UTR, it is likely that this mutation does not disturb expression of the gene. PPR expression was reported to be ubiquitous (Klepikova et al. 2016), and unaltered in response to drought or osmotic stress (Kilian et al. 2007). These results suggest an involvement of pentatricopeptide repeat superfamily protein in the maintenance of rosette growth under control and drought-stress conditions.

In the final locus that we investigated in further detail, the Arabidopsis mutant line targeting xyloglucan endotransglucosylase/transferase 16 (AtXTH16), which is homologous to the gene associated with growth rate under drought stress in cowpea (Fig. 10A), we observed larger ($P < 0.05$; t-test) rosette size under both control and drought conditions (Fig. 10B, Supplementary Fig. S11). Within the cowpea pangenome (Liang et al. 2024) the majority of the sequence variation resides within the gene coding region (five SNPS, Fig. 10A) and 5′ UTR (two SNPs, one indel mutations), however, we could not identify any T-DNA insertions targeting this gene region in Arabidopsis. Expression of AtXTH16 was reported to occur predominantly in the developing leaves of Arabidopsis (Klepikova et al. 2016), and is decreased in the initial stage of drought stress exposure (Kilian et al. 2007). While we could only identify one T-DNA insertion line for this gene, the above results suggest that XTH16 might play a role in rosette growth under control and drought-stress conditions. Overall, we have identified six genes to potentially contribute to drought stress tolerance by maintaining the rosette growth, as increased rosette size was observed in both control and drought-stress conditions (Figs. 8 to 10, Supplementary Fig. S11).

Discussion

Plant phenotyping plays a crucial role in plant breeding, genetic research, and agricultural productivity, and is essential for

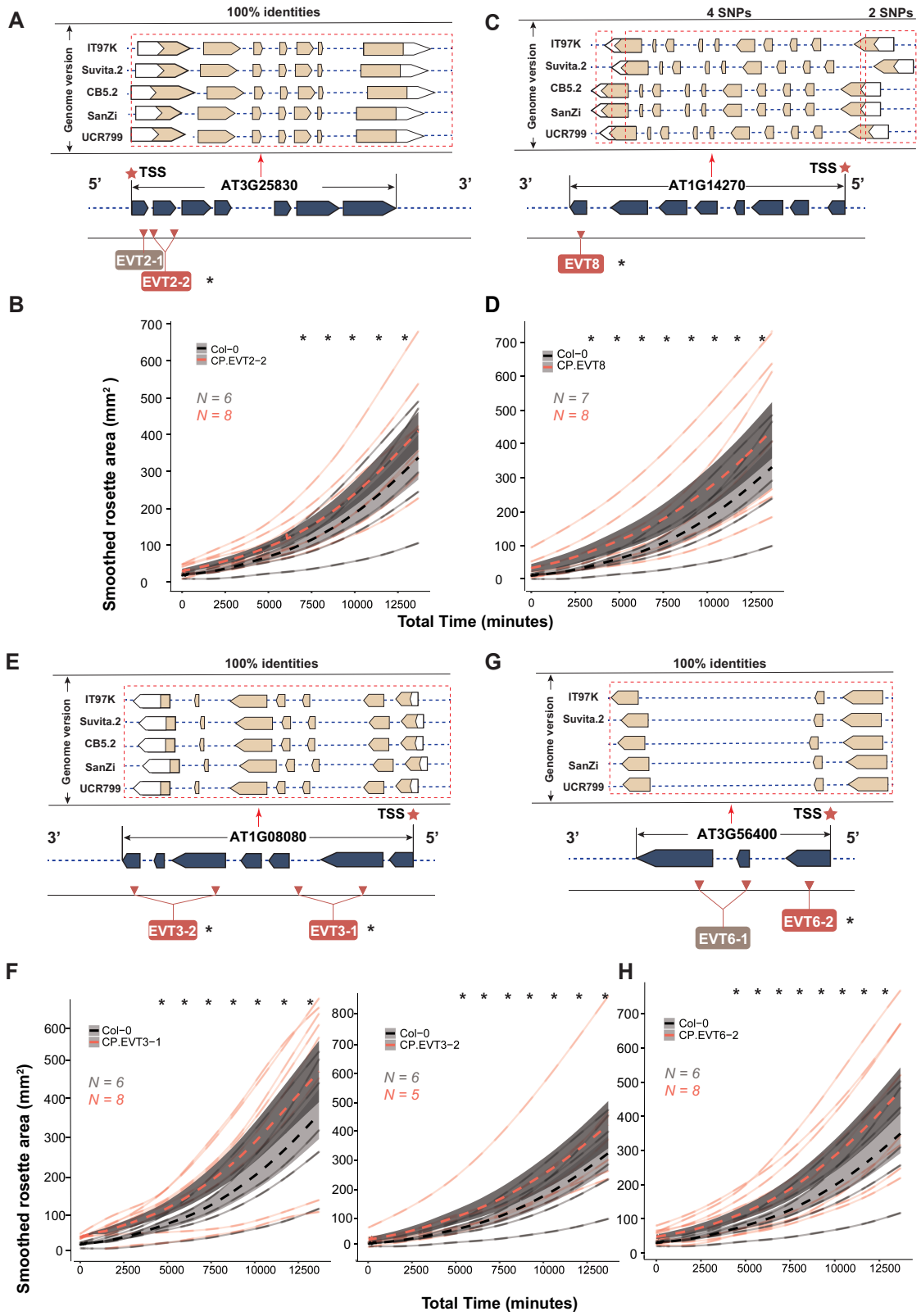

Figure 8. Plant growth of evaporation loci-associated mutants relative to Col-0 plants under drought condition. **A**) Gene model (TSS: transcription start site, marked by red asterisks) of 1,8-cineole synthase (AtTPS27, AT3G25830) and location of EVT2 T-DNA insertion numbers of SNP marked. **B)** Growth of Col-0 and two AtTPS27 mutants under drought conditions with solid lines for each data point, the dashed lines for mean value, and shaded area for standard error (applies to panels **D**, **F**, and **H**). **C)** Gene model of CAAX amino terminal protease (AT1G14270) and location of EVT8 T-DNA insertion. **D**) Growth of Col-0 and protease mutants under drought conditions. **E)** Gene model of alpha carbonic anhydrase 7 (AtACA7, AT1G08080) and the location of EVT3 T-DNA insertions. **F)** Growth of Col-0 and two AtACA7 mutants under drought conditions. **G)** Gene model of AtWRKY70 (AT3G56400) and location of EVT6 T-DNA insertions. **H)** Growth of Col-0 and AtWRKY70 mutant under drought conditions. Only insertion sites with significant differences of leaf area under the drought condition were displayed (t-test: $P < 0.05$).

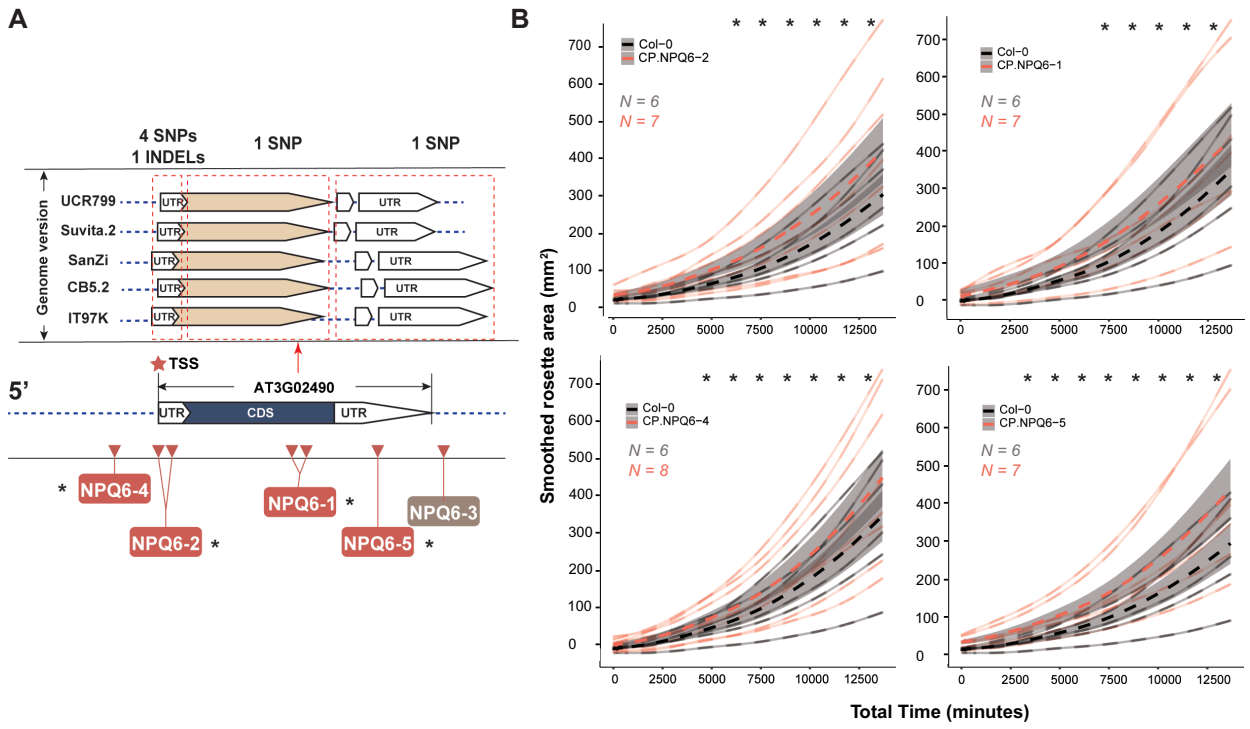

Figure 9. Plant growth of NPQ loci-related mutants relative to Col-0 plants under drought condition. **A**) Gene model (TSS: transcription start site (red asterisk), UTR: untranslated region, and CDS: coding sequences) of pentatricopeptide superfamily protein (AtPPR, AT3G02490) and location of the five T-DNA insertion sites of mutants. In addition, the putative orthologous gene (BLASTN search: *E*-value < 1e05, identities > 95%) from cowpea was identified from five published genome assemblies and gene annotations (UCR799, Suvita.2, SanZi, CB5.2, and IT97K). The multiple-alignment of five putative orthologous genes revealed the high-level conservation across the coding region (1 SNP among five genes), as well as the 3′ UTR (1 SNP) while there were four insertions and deletions (INDELs) identified across the 5′ UTR. **B)** Growth of Col-0 and AtPPR mutants under drought conditions (dashed lines represent mean score and shaded area corresponds to standard error). Only four out of five mutants along with significant differences of leaf area between wild-type and mutants under drought conditions were plotted (*t*-test: *P-value* < 0.05). The significant differences between the wild type (Col-0) and each mutant line were tested using a Student's *t*-test, and *, **, ***, and **** represent *P*-value < 0.05, 0.01, 0.001, and 0.0001 respectively.

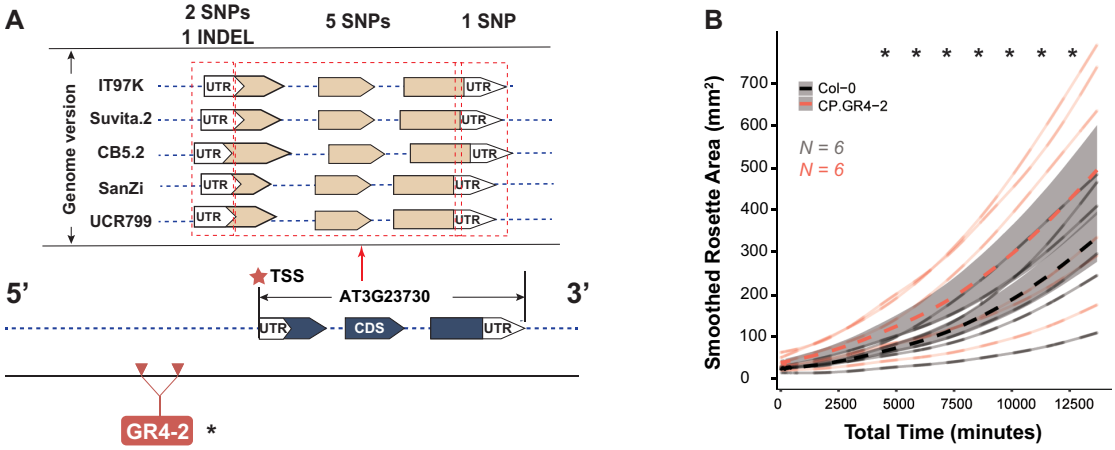

Figure 10. Plant growth of GR loci-related mutants relative to Col-0 plants under drought condition. **A**) Gene model (TSS: transcription start site (red asterisk), UTR: untranslated region, and CDS: coding sequences) of xyloglucan endotransglucosylase/transferase 16 (AtXTH16, AT3G23730) which is associated with growth rate and location of the T-DNA insertion site of one mutant. In addition, the orthologous gene from cowpea was identified from five versions of genome assembly and annotation (UCR799, Suvita.2, SanZi, CB5.2, and IT97K). The multiple alignments of five orthologous genes revealed the different levels of conservation (numbers of SNPs and INDELs across the 5′ UTR (2 SNPs and 1 INDEL), the coding region (5 SNPs), and the 3′ UTR (1 SNP)). **B)** Growth of Col-0 and AtXTH16 mutants under drought conditions (dashed lines represent mean score and shaded area corresponds to standard error). This locus revealed the significant difference in leaf area in between wild-type and mutant (*t*-test: *P*-value < 0.05). The significant differences between the wild type (Col-0) and CP.GR4 mutant line were tested using a Student's *t*-test, and *, **, ***, and **** represent *P*-value < 0.05, 0.01, 0.001, and 0.0001 respectively.

understanding plant growth, development, and responses to the environment. Automated plant phenotyping methods provide valuable information that can be used to improve crop productivity and sustainability, and to address global challenges such as food security and climate change. Implementing computational tools into plant phenotyping enables the efficient processing and analysis of large amounts of images (Fahlgren et al. 2015a; Gehan et al. 2017). As plant phenotyping methods rely on

computational tools, their adoption is often hindered by the requirement of advanced programming skills and the lack of user-friendly interfaces (Klukas et al. 2014; Zhou et al. 2018) Most wet labs consist of scientists with limited programming or engineering experience, and thus it is necessary to democratize the phenotyping tools derived from new technologies and algorithms, and to increase the level of accessibility and convenience of novel tools for the plant scientists.

Here, we present a cost-effective "all-in-one" solution, consisting of three independent cost-effective hardware designs, data processing pipelines, and data analysis platform that streamline individual workflows into one experimental framework (Fig. 3). We aim to break down the bottleneck in plant phenotyping by combining phenotypic image collection with data analysis for users without proficient programming experience. The developed tools allow for navigation between plant images, intermediate datasets, and data analysis. By following the detailed instructions, users can collect data and execute data processing and analysis steps without prior knowledge of engineering.

The most significant advantage of the developed system is its low cost and high versatility. As presented in the results, the hardware pieces were constructed with lightweight and low-cost materials that are simple to assemble (Fig. 1, Supplementary Fig. S2). Moreover, the system's adaptability to a broad range of research contexts was demonstrated by imaging a wide range of plant species. We demonstrated the system's precision by accurately estimating the digital biomass for species grown under controlled environmental conditions (Figs. 3 and 4). AWWEsmo cannot be used to extract transpiration of the plants, but rather evapotranspiration, which is substantially determined by the evaporation of water from the pot (Supplementary Fig. S13). Nevertheless, the device constructed using low-cost materials could adjust the pot weight to the target weight, resulting in reproducible mild drought stress and maintaining soil water-holding capacity throughout the experiment. We would like to note that on-line communities have noted a strong temperature-dependence of the scale sensor precision used within our setup, which would require repeated calibration based on the temperature fluctuations that are commonly observed within growth chamber conditions (Supplementary Fig. S1). In future iterations of AWWEsmo, one might consider replacing the HX711 scale with more reliable weight sensors. Within the described setup, we have checked the scale against a typical laboratory-grade scale for accuracy every week and re-calibrated it if the discrepancy exceeded 1 g. Additionally, as the target weight is not adjusted for the plant size, the described method can only be used for relatively short drought stress experiments. For example, at the end of our cowpea diversity experiment (Fig. 6E), we observed that the evapotranspiration decreased in plants grown under control conditions, probably because they started to experience water limitation. While the difference in leaf temperature was maintained at the end of the experiment (Fig. 6G), we would caution against experiments beyond 2 wk of drought stress using the described method. Similarly, evapotranspiration yields significant associations only when combined with plant fresh weight using the GWAS approach, suggesting that evapotranspiration itself might be too noisy of a trait by itself to be biologically meaningful. Thus, evapotranspiration data derived from AWWEsmo should be treated with caution, and its precision in the current iteration might not be sufficient to detect small evapotranspiration effects for smaller plants, such as Arabidopsis. We would caution anyone to search for additional lines of evidence of plant's water-use to complement the measurements obtained with AWWEsmo. Nevertheless, the accessibility of the developed suite of phenotyping tools provides a starting point for cost-effective phenotyping solutions. The main objective of our system is to monitor plant growth during the early vegetative developmental stage, as this early stage has been the focus of many experiments under controlled conditions (Behmann et al. 2014; Zhang et al. 2020) and RGB image-based phenotyping is reliable in predicting biomass (Rahaman et al. 2017; Banerjee et al. 2020).

The high level of user-friendliness is another feature that characterizes the system. Several published Raspberry Pi-based systems such as "SPIRO", "PhenoBox", and "PhenoWell" are image-based and controlled by low-cost computers for sustainable solutions for high-throughput phenotyping (Czedik-Eysenberg et al. 2018; Feldman et al. 2021; Li et al. 2023; Ohlsson et al. 2024). However, these platforms often rely on R or Python source code for plant objects segmentation, and statistical comparisons, which are making them inflexible for research-based data analysis. In contrast, our developed suite of tools provides not only a comprehensive overview of hardware and software, that has been optimized into reproducible computational pipelines for wider usage but also preserves the flexibility of data analysis that is crucial for research-based use of these tools. To further enable fast and reproducible data analysis, we developed an interactive ShinyApp, RaspiPheno App, to decode plant genotype and treatment information, as well as to perform the data curation, smoothing, and visualization (https://github.com/Leon-Yu0320/BTI-Plant-phenotyping/tree/main/RasPiPheno_APP).

The use of a graphical interface app reduces the downstream workload compared to some other Like other ShinyApps for biological data analysis (Julkowska et al. 2019; Ge 2020; Xiao and Lam 2022). Our efforts enabled that the RaspiPheno App to provide a fast and straightforward approach to data processing. Moreover, the RaspiPheno App offers compatibility with data input derived from previous steps, as it is fine-tuned to match the data output format from the RaspiPheno Pipe. This direct data adoption requires no further data reformatting, reducing the learning curve required for new users. Integration of the RaspiPheno App into the suite of developed tools allows for decoding of information and assigning plant genotype and/or treatment to individual plants, as well as other meta-features of an experimental design. As a result, the streamlined RaspiPheno App enables the acquisition of high-quality plots and systematic statistical analysis of plant growth, to address the specific biological questions about the physiological and genetic basis of plants.

Within this work, we have demonstrated the system's usability using a cowpea diversity panel to drive the discovery of genes involved in environmental resilience. The observed phenotypic variation in cowpea (Fig. 6) was used as an input for GWAS (Fig. 7) to identify genetic loci contributing to drought resilience. Previous studies have identified cowpea as an important donor for drought tolerance traits (Muñoz-Amatriaín et al. 2021), however cowpea phenotyping has thus far not been performed on dynamic traits, such as growth rate or evapotranspiration during drought exposure (Muchero et al. 2009; Verbree et al. 2015; Ravelombola et al. 2020; Nkomo et al. 2022). We observed that similarly to other crop plants (Awlia et al. 2021), cowpea reduces its evapotranspiration (Fig. 6E). On the other hand, the photosynthetic efficiency was only affected in the early phase of drought stress exposure (Fig. 6F). It has been previously reported that Arabidopsis plants under salt stress have been found to decrease quantum yield during early salt stress exposure and that this impacted growth maintenance (Awlia et al. 2021).

To explore the potential genes involved in drought resilience in cowpea, we examined available T-DNA insertion mutants in Arabidopsis homologs to the set of cowpea genes with significant trait associations. Our experiments revealed genes that are potentially contributing to drought resilience (Figs. 8 to 10), highlighting the usefulness of these low-cost, large-scale, phenotyping approaches. Not all studied T-DNA insertion lines showed significant changes in rosette growth rate under drought conditions, and thus require further validation (e.g. AT3G25830 encoding 1,8-cineole synthase, AT1G14270 encoding CAAX amino terminal protease, AT3G56400 encoding AtWRKY70, and AT3G23730 encoding xyloglucan endotransglucosylase/transferase 16, Figs. 8, A to D, G, H and 10). Two out of two studied T-DNA insertion lines targeting alpha carbonic anhydrase 7 (AtACA7, AT1G08080) and four out of five T-DNA insertion lines targeting tetratricopeptide repeat super-family protein (AtPPR, AT3G02490) showed convincing evidence for their potential involvement in drought resilience (Figs. 8, E and F and 9, respectively). Carbonic anhydrases are an abundant protein family that has multiple isoforms and acts in carbon assimilation and photosynthesis (Momayyezi et al. 2020). The three families, alpha, beta, and gamma are considered to have evolved separately (Momayyezi et al. 2020) but have similar functions (Moroney et al. 2001). The alpha carbonic anhydrases have the overall lowest expression level (Polishchuk 2021). While no previous reports cover the role of alpha carbonic anhydrases in drought stress resilience, the beta family has been studied extensively. The expression of beta carbonic anhydrases has been shown to both increase (Polishchuk 2021) and decrease (Wang et al. 2016; Han et al. 2019; Momayyezi et al. 2020) under drought. These contrasting findings, as well as our results, indicate the need for further investigation into the role of alpha carbonic anhydrases in drought response in plants.

PPRs in plants are known for their wide range of molecular functions, including photosynthesis and environmental stress responses, including drought stress Arabidopsis plants exhibited improved growth performance under drought stress when the expression of the PPR protein SLG1 was disrupted (Yuan and Liu 2012). However, Arabidopsis lines overexpressing another PPR protein, SOAR1, also performed better under drought stress compared to the wild type (Jiang and Li 2020). To our knowledge, the PPR identified in this study (AT3G02490) has not been previously studied in detail or reported as contributing to drought resilience. Our previous findings highlight the diversity and complexity of PPR proteins, emphasizing the need to characterize our identified PPR further. The molecular context of these genes will be the focus of future studies, revealing more mechanisms of drought resilience across a wider range of species. Our results illustrate the potential of the developed setup in gene discovery and identification of resilience mechanisms for a wide diversity of plants. In the future, the identified genes can serve as attractive targets for breeding or genetic modification to further contribute to crop stress resilience and food security.

Image-based phenotyping is the workhorse of high-throughput phenotyping (Hall et al. 2022; Langstroff et al. 2022). The application of high-throughput phenotyping in simple and cost-efficient systems, like the one described in our manuscript, carries the potential for a broader impact on plant science research without the prohibitively high costs (Yang et al. 2013; Du et al. 2021; Zhou et al. 2021). The wide adoption of cost-effective solutions can lead to tremendous progress in studying stress responses and identifying genetic components of environmental resilience.

Materials and methods

Phenotyping facility development

Top-view imaging of Arabidopsis using PhenoRig

To continuously collect top-view images, we built a PhenoRig where 32 pots (width: 6.5 cm × length: 6.5 cm × height: 9 cm for each insert), each containing a single Arabidopsis (*A. thaliana*) plant, could be imaged simultaneously within one setup. We built a wooden frame (length: 60 cm × width: 40 cm × height 43.5 cm for the frame) to accommodate a standard 1,020 (~27.94 × 54.61 cm) rectangular tray. The images were collected by two Raspberry Pi cameras connected to a Raspberry Pi Zero computer through an Arducam Multi-camera adapter, with flex cables. To prevent the movement of plants during plant watering, a plastic tray was anchored to the bottom of the PhenoRig. The imaging of plants was performed every 30 min using the automated startup script (described in the pheno-computational pipeline development section below). No additional light source was installed, and the images collected during the night period were removed in the automated data preparation workflow by specifying the start and end time of the light period (hour–minute format: HH:MM) of image collection each day as a parameter input for data allocation (https://github.com/Leon-Yu0320/BTI-Plant-phenotyping). The materials necessary to build a PhenoRig are listed in Supplementary Table S1.

Side-view imaging using PhenoCage

To adequately capture the digital biomass of the plants with complex 3D architectures, such as bean plants, we developed a side-view imaging PhenoCage platform. Within a cage (length: 90 cm × width: 60 cm × height: 60 cm), we placed a rotating platform on which a plant pot is placed. The background noise is limited by white semilight-permeable plastic sheets attached to the frame. The plant is illuminated from four sides and the top using LED light bars to eliminate shading. The light intensity ensures the short shutter speed of the camera, thereby ensuring clear images of the constantly rotating plants. To ensure that all plants will be positioned in the same way on the rotating platform, we attached the pot that has been cut in half in the horizontal direction to the rotating platform. The plants are imaged using one Raspberry Pi camera connected to a Raspberry Pi 4. A household shell script (PhenoCage_capture.sh) takes seven consecutive images, representing a side view of the imaged plant taken every 51.4° (https://github.com/Leon-Yu0320/BTI-Plant-phenotyping/tree/main/data_acquisition). The materials necessary to build a PhenoCage are listed in Supplementary Table S2. Accessories to hold the Raspberry Pi and monitor were designed using TinkerCad (https://www.tinkercad.com) and produced by a 3D printer (PRUSA i3 MK3S+). Examples and details of the 3D printed components can be found at https://github.com/Leon-Yu0320/BTI-Plant-phenotyping/tree/main/3Dprint. While the scale at which the images were taken within the PhenoCage setup within our manuscript constitutes 3 pixels/mm, we kept all the measurements in pixels, as the scale of this setup will depend on the distance between the camera and the plant, that will be specific to individual species studied.

Monitoring evapotranspiration using AWWEsmo

To monitor the plant evapotranspiration, we developed an AWWEsmo. Using this device, the pots are placed on a scale, where they are automatically weighed and watered to their target

weight. We found that the system worked best with the smaller square pots (width: 10.16 cm, length: 10.16 cm, height 11 cm), that were used for cowpea and tepary beans experiments discussed below. The Arduino controller was connected to a load cell (HX711) that served as a scale, and to a submerged 5-V pump that was activated for a period calculated to be necessary to reach the target weight. The controller and the mini-breadboard were placed in a 3D-printed container, designed to protect the electrical components from splatter and dust in the growth chamber. The load cell constituting the scale was attached to the thick plastic platform (thickness: 5 cm, diameter: 12 cm), and a plastic saucer was glued to the platform, to prevent water spillage onto the electrical components. The Arduino controller as well as the load cell were housed in a 3D-printed design, that accommodated two levelers, ensuring the scale leveling and support for the hose connected to the pump. The materials necessary to build an AWWEsmo device are listed in Supplementary Table S3, while detailed instructions on how to build and program the device can be found at https://github.com/ok84-star/AAWSMO. Details on the 3D-printed designs can be found at https://github.com/Leon-Yu0320/BTI-Plant-phenotyping/tree/main/3Dprint/AWESmo. The detailed usage manual, including calibration and execution of the AWWEsmo, is available at protocols.io (Julkowska et al. 2023; Khmelnitsky et al. 2023). Supplemental Video on assembly can be found here: https://youtu.be/QlJUVdQT6VA. The precision of the load cell was evaluated against a laboratory scale (Kern EMB portable balance) to 0.1 g precision. The Arduino scale was calibrated prior to every experiment using the scripts available at https://github.com/ok84-star/AAWSMO and checked during each measurement against the laboratory scale mentioned previously.

Pheno-computational pipeline development

The plant image collection is integrated into a customizable shell script, optimized for ISO, image sharpness (sh), contrast (co), brightness (br), shutter speed (ss), and size of the image for individual imaging conditions. For the PhenoRig setup, the automated data collection was conducted with specifications of time interval (unit: min), duration (unit: days), and hardware identifiers (format: RaspiID_cameraID). Once the image and experimental settings are determined by the user, the imaging command is deployed at determined time intervals using crontab which is nested within the setup scripts. Users can launch the collection by using a local Raspi computer, or connect Raspi computers to the internet and launch the program remotely by a personal computer (PC) or a server. For PhenoCage setup, image data collection is launched manually for individual plants. For each plant, images from seven sides were collected with a hardware identifier (format: RaspiID) and side numbers (format: side1 to side7). After each experiment session for both PhenoRig and PhenoCage, images can be transferred using a USB flash drive or an SSH transfer proxy to a server or other local devices.

After image collection, the pipeline requires experiment-specific parameters as input to execute the image analysis correctly. The parameters guide key steps related to image transformation, masking, selection of regions of interest, and extraction of phenotypic data into an image analysis protocol derived from PlantCV image processing algorithm (Gehan et al. 2017), a tutorial for parameter setup for PlantCV software was instructed using example images collected with PhenoRig and PhenoCage (Yu and Julkowska 2022). The computation pipelines and RasPiPheno Pipe are publicly available on GitHub with manual and supplementary information provided (https://github.com/Leon-Yu0320/BTI-Plant-phenotyping).

The quantitative data obtained from collected images are subsequently analyzed for changes in digital biomass throughout time/treatment. Prior to statistical data analysis, data collected using PhenoCage is additionally processed by summarizing the pixels representing the shoot projected area from seven side-view images. Once the digital biomass of each plant is determined from either side-view or top-view images, the genotype, replicate, and treatment information is decoded using a meta-data table (https://github.com/Leon-Yu0320/BTI-Plant-phenotyping/tree/main/Results_example). While PhenoRig images are decoded based on positional information, the PhenoCage data is decoded based on the timestamp of the image, assuming that the experiment is imaged sequentially in order of the pot position. The decoded data is subsequently processed under the framework RasPiPhenoApp (https://github.com/Leon-Yu0320/BTI-Plant-phenotyping), a web interactive and streamlined analysis tool. Using the smooth spline, loess fit, or polynomial regression fit functions, each data point is curated to generate curated values as a smoothed dataset. The original data points that exceed the one to three times standard deviation (SD) relative to corresponding curated values can be classified as outliers. The user can remove specific points based on the customized cutoff (one to three times SD), to generate a clean dataset. The growth rates (GR) are calculated using a linear function either for the entire duration of the experiment (PhenoCage) or for each day of the experiment (PhenoRig). The differences between treatments and/or genotypes (or in other single factors, two factors experiments) are subsequently tested using *t*-test, Wilcox, ANOVA, or two-way ANOVA regarding the curated plant leaf area, the leaf area without outliers, and growth rate. The visualization of the graphs is performed using ggplot2 and ggpubr packages (Wickham 2016). The integration of data analysis tools into a graphical user interface is performed using *shiny* R package (https://shiny.rstudio.com).

Plant material and plant growth conditions

Arabidopsis thaliana experiment

Arabidopsis (*A. thaliana*) Col-0 seeds were sterilized for 10 min with 50% (v/v) bleach and rinsed five times using Milli-Q water and germinated on ½ strength × Murashige and Skoog (MS) medium containing 0.5% (w/v) sucrose, 0.1% (w/v) 4-morpholineethanesulfonic acid (MES), and 1% (w/v) agar. After 24 h of vernalization at 4 °C in the dark, the plates were placed in the Conviron growth chamber with the light intensity of 130 to 150 μmol m^{-2} s^{-1} in a 16 h light/8 h dark cycle at 21 °C and 60% humidity. At 7 d after germination, the seedlings were transplanted to soil (Cornell Mix, per batch combine: 0.16 m^3 of peat moss, 20.84 kg of vermiculite, 0.59 kg of Uni-Mix fertilizer, and 2.27 kg of lime) watered to 100% soil water-holding capacity and placed in a walk-in growth chamber with the abovementioned conditions. When the pots dried to the weight corresponding to 50% of their water holding capacity, they were soaked for 1 h in tap water or a 200 mM NaCl solution, resulting in a concentration of 100 mM NaCl based on the 50% soil water holding capacity, which corresponded to a moderate level of salt stress according to (Awlia et al. 2021). We allowed the pots to be drained for 2 to 3 h to eliminate excess moisture. The pots were subsequently placed under PhenoRigs equipped with an automated imaging system, and the pot weight was measured and adjusted daily to maintain the reference weight corresponding to 50% of the soil water-holding

capacity throughout the experiment. At the end of the experiment, fresh weight was collected for all imaged plants. The collected images were processed using the pheno-computational pipeline described above, and the data were processed in R (Supplementary Table SS4). All the data was tested for ANOVA assumptions, including homogeneity of variance and normal distribution using MVApp (Julkowska et al. 2019).

Cowpea pilot experiment

The seeds of five cowpea accessions (CB5-2, IT97K-499, Sanzi, Suvita-2, UCR799), representative of the wider diversity within cowpea were germinated in square pots (width: 10.16 cm; length: 10.16 cm, height: 11 cm) filled with soil (Cornell Mix + Osmocote, composed of Cornell Mix mentioned above with 2.27 kg Osmocote added per 1.631 m^3) (Liang et al. 2024). The plants were germinated and grown in a Conviron growth chamber with the light intensity at 350 to 415 μmol m^{-2} s^{-1} under a 12 h light cycle at 26 °C/12 h dark cycle at 20 °C and 50% relative humidity. We calculated vapor pressure deficit (VPD) using the R package "plantecophys" (Duursma 2015). The daytime VPD was 1.17 kPa and the nighttime VPD was 1.69 kPa. No additional nutrients were added during the experiment. We used seven biological replicates per accession per treatment for this experiment. The control and drought-treated plants were kept at 60% and 20% soil water-holding capacity, respectively. To determine target weights for each pot, we left the pots to air dry for 72 h and assigned this weight to correspond to 0% water-holding capacity. We then saturated the soil for 24 h, removed excess water, weighed the pots, and assigned this value as the 100% soil water-holding capacity weight. At this point, we sowed two seeds per pot and thinned it to one seedling per pot after germination occurred. We initiated tracking pot weight at 17 d after germination, watering each pot to its target weight daily for 15 consecutive days. Drought treatment target weights were reached on day 4 after tracking started. We imaged the plants using the PhenoCage setup starting 17 d after germination and subsequently every other day for the next 2 wk (resulting in a total of seven-time points, with each time point consisting of seven images for each plant). At the end of the experiment, the fresh weight of the cowpea shoot was collected for all the imaged plants. The collected images were processed using the pheno-computational pipeline described above, and the data was processed in R (Supplementary Table S4). All of the data was tested for ANOVA assumptions, including homogeneity of variance and normal distribution using MVApp (Julkowska et al. 2019).

Tepary bean pilot experiment

The seeds of twp tepary bean accessions (TDP359 and TDP22), representative of the wild and cultivated tepary bean, respectively (Muñoz-Amatriaín et al. 2021), were germinated in 4-in. pots filled with soil (Cornell Mix + Osmocote) watered to 100% soil water-holding capacity. We used six biological replicates of TDP359 (cultivated) and 12 replicates of TDP22 (wild) per treatment for this experiment. The control and drought-treated plants were kept at 60% and 10% soil water-holding capacity, respectively. The drought was imposed as described for the cowpea pilot experiment above and the growth chamber conditions were the same as for the cowpea pilot experiment, described above. We imaged the plants using the PhenoCage setup starting at 17 d after germination and repeated every second day for consecutive 2 wk. At the end of the experiment, the fresh weight of the tepary bean shoot was collected for all the imaged plants. The collected images were processed using the pheno-computational pipeline described above, and the data was processed in R (Supplementary Table S4). All the data was tested for ANOVA assumptions, including homogeneity of variance and normal distribution using MVApp (Julkowska et al. 2019).

Cowpea mini-core population screen

The cowpea mini-core population, consisting of 368 accessions (Muñoz-Amatriaín et al. 2021) was screened as described for the cowpea pilot experiments. The accessions were distributed over six experiments, and we used five accessions (CB5-2, IT97K-499, Sanzi, Suvita-2, and UCR799) as internal standards for each experiment. One accession, TVu-9393 was excluded because it did not germinate after multiple trials, and another accession, TVu-3965, was omitted due to lack of seeds available. The drought imposition and growth chamber conditions were the same as described for the cowpea pilot experiment in the above sections. The pot weight was monitored and adjusted every day, while imaging of the plants using PhenoCage was performed every second day. Due to the various growth habits of cowpeas, we occasionally added transparent, 3D-printed support to ensure the upright position of the plant. The weight of the support was accounted for in the evapotranspiration data analysis. Additionally, we measured photosynthetic efficiency, leaf temperature, and chlorophyll content using the PhotoSynQ device at 6 and 13 d after treatment initiation. At the end of each experiment, the fresh weight of the cowpea shoot tissue was collected for all the imaged plants. The collected images were processed using the pheno-computational pipeline described above. This dataset includes six sets of experiments, evaporation rate curation for individual plants, and the side-view image data comparison derived per experiment was performed using the R scripts (Supplementary Table S4). Subsequently, individual experimental data were merged, modeled using smooth splines, used to calculate growth rate and cumulative evapotranspiration per gram of fresh weight, and prepared for subsequent GWAS (Supplementary Table S4). The raw and curated data can be accessed in open-access Zenodo Repositories (overview and links are listed in Supplementary Tables S5 to S7). All of the data was tested for ANOVA assumptions, including homogeneity of variance and normal distribution using MVApp (Julkowska et al. 2019).

GWAS of drought stress responses in cowpea

All collected and curated phenotypic data were used for GWAS. The kinship matrix was calculated for all included accessions using GAPIT (Wang and Zhang 2021), and included as a co-factor in the GWAS mixed model (https://github.com/arthurkorte/GWAS). The GWAS model uses fast approximation (Zhang and Liu 2011) and relies on the ASReml library (Butler et al. 2009). The results files were subsequently processed to draw QQ-plots, indicating any bias within the GWAS model, Manhattan plots to identify significant associations above the Bonferroni threshold, as well as the effect size plots to evaluate the estimated effect size of the loci selected for further inspection (Supplementary Table S4). The identified genomic regions were compared between the traits mapped under control and drought stress conditions (Supplementary Table S8). Loci identified exclusively under drought stress conditions were considered for further evaluation. The GWAS output files, as well as all the generated plots, can be accessed in open-access Zenodo Repository (https://doi.org/10.5281/zenodo.7438567).

Screening of homologs in Arabidopsis for their contribution to drought resilience

The drought-specific loci identified through cowpea GWAS described above were investigated for annotated genes within the linkage disequilibrium (LD, 30 kbp) of the identified SNP. Arabidopsis sequence homologs to the genes within the LD were acquired from the cowpea genome annotation (Lonardi et al. 2019). For each identified Arabidopsis homolog, we explored publicly available homozygous T-DNA insertion lines that exclusively target our gene of interest. The lines and their corresponding cowpea genes are listed in Supplementary Table S9. The seeds were ordered from ABRC (https://abrc.osu.edu/), and the seeds of each mutant line were grown alongside the Col-0 genotype, as described for the Arabidopsis phenotyping experiment above. Two weeks after germination, the seedlings were exposed to control or drought stress conditions (60% and 10% of soil water-holding capacity, respectively). The plants were monitored for growth using the PhenoRig setup every 30 min, while evapotranspiration of every plant was monitored every 48 h using the AWWEsmo device. Based on the results and phenotypes of mutants with significantly affected growth rates under drought stress, we made a selection of 14 T-DNA insertion lines for further evaluation (CP.GR4-1, CP.GR4-2, CP.NPQ6-1, CP.NPQ6-2, CP.NPQ6-3, CP.NPQ6-4, CP.NPQ6-5, CP.EVT2-1, CP.EVT2-2, CP.EVT3-1, CP.EVT3-2, CP.EVT6-1, CP.EVT6-2, CP.EVT8, Supplementary Table S9). One hundred percent water-holding capacity was determined as described above for the Cowpea Pilot Experiment. Concurrently, we grew the 14 T-DNA insertion lines on ½ MS plates for 10 d and transferred the seedlings to the soil. Two weeks after germination, we initiated tray imaging every 30 min. To efficiently bring the drought treatment pots down to 20% water-holding capacity, we placed small fans above them for a 90-min increment. The setup to induce drought stress is depicted within Supplementary Fig. S14. Seventeen days after germination, we began tracking water-use every second day, and this day was marked as day 1 of stress. Images were taken for 2 wk. Primary bolts were cut from plants that began flowering within these 2 wk to prevent bias in the image analysis. The data was analyzed in the same way as described in previous experiments. The specific R markdown files and raw dataset can be accessed at https://github.com/Leon-Yu0320/BTI-Plant-phenotyping/tree/main/ImageData_curation_example.

Accession numbers

The list of specific mutant lines used in this study including their accession number is listed in Supplementary Table S9.

Acknowledgments

We would like to thank the BTI workshop team, Lucas Burke and Don Slocum, for their help in setting up the wooden frames for the PhenoRigs and PhenoCages. We would like to acknowledge Ms. Holly Carter and Ms. Rose Deshler (2021 REU students) for their help in troubleshooting data acquisition on the PhenoRigs. The authors would also like to acknowledge Dr. Maria Munoz-Amatrain for sharing the population of the cowpea miniCORE diversity panel.

Author contributions

M.M.J. designed the research; H.S., L.Y., M.R.I., O.K., and A.S. performed the research; L.Y., O.K., M.M.J., and A.N. contributed new analytic and computational tools; L.Y., H.S., A.S., and M.M.J. analyzed the data; M.M.J., L.Y., and H.S. wrote the paper, and all of the authors reviewed it.

Supplementary data

The following materials are available in the online version of this article.

Supplementary Figure S1. Precision of AWWEsmo system.
Supplementary Figure S2. Components of PhenoRig and PhenoCage system.
Supplementary Figure S3. The 3D printed accessories used for phenotyping.
Supplementary Figure S4. Construction of the imaging trellis for tepary beans.
Supplementary Figure S5. Drought-induced changes in evapotranspiration of cowpea and tepary beans.
Supplementary Figure S6. The effects of drought on evapotranspiration in cowpeas.
Supplementary Figure S7. First experimental batch of drought-induced changes in daily growth rate among Arabidopsis T-DNA insertion lines.
Supplementary Figure S8. Second experimental batch of drought-induced changes in daily growth rate among Arabidopsis T-DNA insertion lines.
Supplementary Figure S9. Drought-induced changes in evapotranspiration, leaf temperature, and NPQ among Arabidopsis T-DNA insertion lines.
Supplementary Figure S10. Evapotranspiration of mutants versus Col-0 of NPQ-related loci.
Supplementary Figure S11. The leaf rosette area of studied *Arabidopsis* mutant lines under nonstress conditions.
Supplementary Figure S12. The leaf rosette area of studied Arabidopsis mutant lines under drought conditions.
Supplementary Figure S13. Evapotranspiration of empty pots.
Supplementary Figure S14. The fan setup for imposing lower soil water-holding capacity in Arabidopsis seedlings.
Supplementary Table S1. PhenoRig construction materials.
Supplementary Table S2. PhenoCage construction materials.
Supplementary Table S3. AWEsmo construction materials.
Supplementary Table S4. Description and link of R notebooks.
Supplementary Table S5. Description and link of repositories of datasets.
Supplementary Table S6. Mean Genotype Growth Rates for each condition.
Supplementary Table S7. The genotypic means for each accessions used as input for GWAS.
Supplementary Table S8. Associations in cowpea miniCORE population identified through GWAS.
Supplementary Table S9. The list of GWAS candidate genes, their Arabidopsis homologs and mutant lines used within this study.

Funding

The work is supported by USDA National Institute of Food and Agriculture grant number 2022-67013-36212 (to M.M.J.). The authors want to acknowledge NSF-IOS 2023310 and 2102120 (to A.D.L.N.). The work on developing affordable phenotyping systems has been supported through Goelet Foundation.

Conflict of interest statement. None declared.

Data availability

Links associated with all image data derived from Raspi PhenoRig, PhenoCage, and AWWESmo can be accessed under Supplementary Table SS5. Video tutorial for using the

RaspiPheno App can be reached at https://www.youtube.com/channel/UCnO5hHc-h6Ms-vlg3_IFQSw.

References

Abbasi A, Fahlgren N. Naive Bayes pixel-level plant segmentation. Conference: 2016 IEEE Western New York Image and Signal Processing Workshop (WNYISPW). Rochester (NY): IEEE Xplore; 2016. https://doi.org/10.1109/WNYIPW.2016.7904790

Akashi K, Miyake C, Yokota A. Citrulline, a novel compatible solute in drought-tolerant wild watermelon leaves, is an efficient hydroxyl radical scavenger. *FEBS Lett*. 2001:508:438–442. https://doi.org/10.1016/s0014-5793(01)03123-4

Alberto Gutierrez Ortega J, Fahlgren N, Gehan M, Castillo. Segmentation of overlapping plants in multi-plant image time series. *ESS Open Archive*. 2021. https://doi.org/10.1002/essoar.10508337.2

Awlia M, Alshareef N, Saber N, Korte A, Oakey H, Panzarová K, Trtílek M, Negrão S, Tester M, Julkowska MM. Genetic mapping of the early responses to salt stress in *Arabidopsis thaliana*. *Plant J*. 2021:107(2):544–563. https://doi.org/10.1111/tpj.15310

Awlia M, Nigro A, Fajkus J, Schmoeckel SM, Negrão S, Santelia D, Trtílek M, Tester M, Julkowska MM, Panzarová K. High-throughput non-destructive phenotyping of traits that contribute to salinity tolerance in Arabidopsis thaliana. *Front Plant Sci*. 2016:7:1414. https://doi.org/10.3389/fpls.2016.01414

Banerjee BP, Joshi S, Thoday-kennedy E, Pasam RK, Tibbits J, Hayden M, Spangenberg G, Kant S. High-throughput phenotyping using digital and hyperspectral imaging-derived biomarkers for genotypic nitrogen response. *J Exp Bot*. 2020:71(15):4604–4615. https://doi.org/10.1093/jxb/eraa143

Behmann J, Steinrücken J, Plümer L. Detection of early plant stress responses in hyperspectral images. *ISPRS J Photogramm Remote Sens*. 2014:93:98–111. https://doi.org/10.1016/j.isprsjprs.2014.03.016

Berry JC, Fahlgren N, Pokorny AA, Bart RS, Veley KM. An automated, high-throughput method for standardizing image color profiles to improve image-based plant phenotyping. *PeerJ*. 2018:6:e5727. https://doi.org/10.7717/peerj.5727

Bethge H, Winkelmann T, Lüdeke P, Rath T. Low-cost and automated phenotyping system "Phenomenon" for multi-sensor in situ monitoring in plant in vitro culture. *Plant Methods*. 2023:19:42. https://doi.org/10.1186/s13007-023-01018-w

Brady SM, Orlando DA, Lee J-Y, Wang JY, Koch J, Dinneny JR, Mace D, Ohler U, Benfey PN. A high-resolution root spatiotemporal map reveals dominant expression patterns. *Science*. 2007:318:801–806. https://doi.org/10.1126/science.1146265

Butler D, Cullis B, Gilmour A, Gogel B. Analysis of mixed models for S–language environments: ASReml–R reference manual. Hemel Hempstead, UK: VSN International Ltd; 2009. p. 160.

Casto A, Schuhl H, Fahlgren N, Gehan M, Schneider D, Wheeler J. Analyzing chlorophyll fluorescence images in PlantCV. *ESS Open Archive*. 2022. https://doi.org/10.1002/essoar.10508322.3

Chawade A, Van Ham J, Blomquist H, Bagge O, Alexandersson E, Ortiz R. High-throughput field-phenotyping tools for plant breeding and precision agriculture. *Agronomy*. 2019:9:258. https://doi.org/10.3390/agronomy9050258

Chen F, Ro DK, Petri J, Gershenzon J, Bohlmann J, Pichersky E, Tholl D. Characterization of a root-specific *Arabidopsis* terpene synthase responsible for the formation of the volatile monoterpene 1,8-cineole. *Plant Physiol*. 2004:135(4):1956–1966. https://doi.org/10.1104/pp.104.044388

Choudhury S, Moulick D, Ghosh D, Soliman M, Alkhedaide A, Gaber A, Hossain A. Drought-induced oxidative stress in pearl millet (*Cenchrus americanus* L.) at seedling stage: survival mechanisms through alteration of morphophysiological and antioxidants activity. *Life (Basel)*. 2022:23(8):1171. https://doi.org/10.3390/life12081171

Colmer J, O'Neill CM, Wells R, Bostrom A, Reynolds D, Websdale D, Shiralagi G, Lu W, Lou Q, Le Cornu T, *et al*. SeedGerm: a cost-effective phenotyping platform for automated seed imaging and machine-learning based phenotypic analysis of crop seed germination. *New Phytol*. 2020:228(2):778–793. https://doi.org/10.1111/nph.16736

Correa J, Postma JA, Watt M, Wojciechowski T. Soil compaction and the architectural plasticity of root systems. *J Exp Bot*. 2019:70:6019–6034. https://doi.org/10.1093/jxb/erz383

Cullis C, Kunert KJ. Unlocking the potential of orphan legumes. *J Exp Bot*. 2017:68:1895–1903. https://doi.org/10.1093/jxb/erw437

Czedik-Eysenberg A, Seitner S, Güldener U, Koemeda S, Jez J, Colombini M, Djamei A. The 'PhenoBox', a flexible, automated, open-source plant phenotyping solution. *New Phytol*. 2018:219(2):808–823. https://doi.org/10.1111/nph.15129

Das Choudhury S, Samal A, Awada T. Leveraging image analysis for high-throughput plant phenotyping. *Front Plant Sci*. 2019:10:508. https://doi.org/10.3389/fpls.2019.00508

Dhondt S, Gonzalez N, Blomme J, De Milde L, Van Daele T, Van Akoleyen D, Storme V, Coppens F, T S Beemster G, Inzé D. High-resolution time-resolved imaging of in vitro Arabidopsis rosette growth. *Plant J*. 2014:80(1):172–184. https://doi.org/10.1111/tpj.12610

Du J, Fan J, Wang C, Lu X, Zhang Y, Wen W, Liao S, Yang X, Guo X, Zhao C. Greenhouse-based vegetable high-throughput phenotyping platform and trait evaluation for large-scale lettuces. *Comput Electron Agric*. 2021:186:106193. https://doi.org/10.1016/j.compag.2021.106193

Duursma RA. Plantecophys – an R package for analysing and modelling leaf gas exchange data. *PLoS One*. 2015:10(11):e0143346. https://doi.org/10.1371/journal.pone.0143346

Ellison Mathe S, Bandaru M, Kishan Kondaveeti H, Vappangi S, Sanjiv Rao G. A survey of agriculture applications utilizing raspberry Pi. 2022 International Conference on Innovative Trends in Information Technology, ICITIIT 2022. Kottayam, India: IEEE; 2022. https://doi.org/10.1109/ICITIIT54346.2022.9744152

Fahlgren N, Feldman M, Gehan MA, Wilson MS, Shyu C, Bryant DW, Hill ST, McEntee CJ, Warnasooriya SN, Kumar I, *et al*. A versatile phenotyping system and analytics platform reveals diverse temporal responses to water availability in *Setaria*. *Mol Plant*. 2015a:8-(10):1520–1535. https://doi.org/10.1016/j.molp.2015.06.005

Fahlgren N, Gehan MA, Baxter I. Lights, camera, action: high-throughput plant phenotyping is ready for a close-up. *Curr Opin Plant Biol*. 2015b:24:93–99. https://doi.org/10.1016/j.pbi.2015.02.006

Feldman A, Wang H, Fukano Y, Kato Y, Ninomiya S, Guo W. EasyDCP: an affordable, high-throughput tool to measure plant phenotypic traits in 3D. *Methods Ecol Evol*. 2021:12(9):1679–1686. https://doi.org/10.1111/2041-210X.13645

Fiorani F, Schurr U. Future scenarios for plant phenotyping. *Annu Rev Plant Biol*. 2013:64(1):267–291. https://doi.org/10.1146/annurev-arplant-050312-120137

Furbank RT, Tester M. Phenomics—technologies to relieve the phenotyping bottleneck. *Trends Plant Sci*. 2011:16(12):635–644. https://doi.org/10.1016/j.tplants.2011.09.005

Ge SX, Jung D, Yao R. ShinyGO: a graphical gene-set enrichment tool for animals and plants. *Bioinformatics*. 2020:36(8):2628–2629. https://doi.org/10.1093/bioinformatics/btz931

Gehan MA, Fahlgren N, Abbasi A, Berry JC, Callen ST, Chavez L, Doust AN, Feldman MJ, Gilbert KB, Hodge JG, *et al*. PlantCV v2: image

analysis software for high-throughput plant phenotyping. *PeerJ*. 2017:5:e4088. https://doi.org/10.7717/peerj.4088

Godin C. Representing and encoding plant architecture: a review. *Ann For Sci*. 2000:57(5):413–438. https://doi.org/10.1051/forest:2000132

Grieder C, Trachsel S, Hund A. Early vertical distribution of roots and its association with drought tolerance in tropical maize. *Plant Soil*. 2014:377(1-2):295–308. https://doi.org/10.1007/s11104-013-1997-1

Hairmansis A, Berger B, Tester M, Roy SJ. Image-based phenotyping for non-destructive screening of different salinity tolerance traits in rice. *Rice (N Y)*. 2014:7(1):16. https://doi.org/10.1186/s12284-014-0016-3

Hall RD, D'Auria JC, Silva Ferreira AC, Gibon Y, Kruszka D, Mishra P, van de Zedde R. High-throughput plant phenotyping: a role for metabolomics? *Trends Plant Sci*. 2022:27(6):549–563. https://doi.org/10.1016/j.tplants.2022.02.001

Han J, Lei Z, Zhang Y, Yi X, Zhang W, Zhang Y. Drought-introduced variability of mesophyll conductance in Gossypium and its relationship with leaf anatomy. *Physiol Plant*. 2019:166(3):873–887. https://doi.org/10.1111/ppl.12845

Harrison MT, Tardieu F, Dong Z, Messina CD, Hammer GL. Characterizing drought stress and trait influence on maize yield under current and future conditions. *Glob Chang Biol*. 2014:20(3):867–878. https://doi.org/10.1111/gcb.12381

Hodge JG, Li Q, Doust AN. De novo homology assessment from landmark data: a workflow to identify and track segmented structures in plant time series images. bioRxiv 029983. https://doi.org/10.1101/2021.02.21.432162, 22 February 2021, preprint: not peer reviewed.

Hughes J, Hepworth C, Dutton C, Dunn JA, Hunt L, Stephens J, Waugh R, Cameron DD, Gray JE. Reducing stomatal density in barley improves drought tolerance without impacting on yield. *Plant Physiol*. 2017:174(2):776–787. https://doi.org/10.1104/pp.16.01844

Jiang Y, Li C. Convolutional neural networks for image-based high-throughput plant phenotyping: a review. *Plant Phenomics*. 2020:2020:4152816. https://doi.org/10.34133/2020/4152816

Julkowska MM, Khmelnitsky O, Sussman H, Khmelnitsky O, Khmelnitsky O. Loading and execution of automatic watering and weighing. *protocol.io*. 2023:1–7.

Julkowska MM, Saade S, Agarwal G, Gao G, Pailles Y, Morton M, Awlia M, Tester M. MVApp—multivariate analysis application for streamlined data analysis and curation. *Plant Physiol*. 2019:180(3):1261–1276. https://doi.org/10.1104/pp.19.00235

Khmelnitsky O, Julkowska MM, Sussman H, Khmelnitsky O. Calibration protocol code and uploading. *protocol.io*. 2023:1–5.

Kilian J, Whitehead D, Horak J, Wanke D, Weinl S, Batistic O, D'Angelo C, Bornberg-Bauer E, Kudla J, Harter K. The AtGenExpress global stress expression data set: protocols, evaluation and model data analysis of UV-B light, drought and cold stress responses. *Plant J*. 2007:50(2):347–363. https://doi.org/10.1111/j.1365-313X.2007.03052.x

Klepikova AV, Kasianov AS, Gerasimov ES, Logacheva MD, Penin AA. A high resolution map of the Arabidopsis thaliana developmental transcriptome based on RNA-seq profiling. *Plant J*. 2016:88(6):1058–1070. https://doi.org/10.1111/tpj.13312

Klukas C, Chen D, Pape J. Integrated analysis platform: an open-source information system for high-throughput plant phenotyping. *Plant Physiol*. 2014:165(2):506–518. https://doi.org/10.1104/pp.113.233932

Koitabashi R, Suzuki T, Kawazu T, Sakai A, Kuroiwa H, Kuroiwa T. 1,8-Cineole inhibits root growth and DNA synthesis in the root apical meristem of *Brassica campestris* L. *J Plant Res*. 1997:110(1):1–6. https://doi.org/10.1007/BF02506836

Kolhar S, Jagtap J. Phenomics for Komatsuna plant growth tracking using deep learning approach. *Expert Syst Appl*. 2023:215:119368. https://doi.org/10.1016/j.eswa.2022.119368

Kondaveeti HK, Bandi D, Mathe SE, Vappangi S, Subramanian M. A review of image processing applications based on raspberry-Pi. 8th International Conference on Advanced Computing and Communication Systems, ICACCS 2022. Coimbatore, India: IEEE; 2022. p. 22–28.

Langstroff A, Heuermann MC, Stahl A, Junker A. Opportunities and limits of controlled-environment plant phenotyping for climate response traits. *Theor Appl Genet*. 2022:135(1):1–6. https://doi.org/10.1007/s00122-021-03892-1

Li J, Mintgen MAC, D'Haeyer S, Helfer A, Nelissen H, Inzé D, Dhondt S. PhenoWell—a novel screening system for soil-grown plants. *Plant Environ Interact*. 2023:4(2):55–69. https://doi.org/10.1002/pei3.10103

Liang Q, Muñoz-Amatriaín M, Shu S, Lo S, Wu X, Carlson JW, Davidson P, Goodstein DM, Phillips J, Janis NM, *et al*. A view of the pan-genome of domesticated Cowpea (*Vigna unguiculata* [L.] Walp.). *Plant Genome*. 2024:17(1):e20319. https://doi.org/10.1002/tpg2.20319

Lonardi S, Muñoz-Amatriaín M, Liang Q, Shu S, Wanamaker SI, Lo S, Tanskanen J, Schulman AH, Zhu T, Luo MC, *et al*. The genome of cowpea (Vigna unguiculata [L.] Walp.). *Plant J*. 2019:98(5):767–782. https://doi.org/10.1111/tpj.14349

Marchetti CF, Ugena L, Humplík JF, Polák M, Ćavar Zeljković S, Podlešáková K, Fürst T, De Diego N, Spíchal L. A novel image-based screening method to study water-deficit response and recovery of barley populations using canopy dynamics phenotyping and simple metabolite profiling. *Front Plant Sci*. 2019:10:1252. https://doi.org/10.3389/fpls.2019.01252

Meza I, Siebert S, Döll P, Kusche J, Herbert C, Eyshi Rezaei E, Nouri H, Gerdener H, Popat E, Frischen J, *et al*. Global-scale drought risk assessment for agricultural systems. *Nat Hazards Earth Syst Sci*. 2020:20(2):695–712. https://doi.org/10.5194/nhess-20-695-2020

Minervini M, Giuffrida MV, Perata P, Tsaftaris SA. Phenotiki: an open software and hardware platform for affordable and easy image-based phenotyping of rosette-shaped plants. *Plant J*. 2017:90(1):204–216. https://doi.org/10.1111/tpj.13472

Momayyezi M, McKown AD, Bell SCS, Guy RD. Emerging roles for carbonic anhydrase in mesophyll conductance and photosynthesis. *Plant J*. 2020:101(4):831–844. https://doi.org/10.1111/tpj.14638

Moroney JV, Bartlett SG, Samuelsson G. Carbonic anhydrases in plants and algae: invited review. *Plant Cell Environ*. 2001:24(2):141–153. https://doi.org/10.1111/j.1365-3040.2001.00669.x

Muchero W, Ehlers JD, Close TJ, Roberts PA. Mapping QTL for drought stress-induced premature senescence and maturity in cowpea [*Vigna unguiculata* (L.) Walp.]. *Theor Appl Genet*. 2009:118(5):849–863. https://doi.org/10.1007/s00122-008-0944-7

Muñoz-Amatriaín M, Lo S, Herniter IA, Boukar O, Fatokun C, Carvalho M, Castro I, Guo YN, Huynh BL, Roberts PA, *et al*. The UCR Minicore: a resource for cowpea research and breeding. *Legume Sci*. 2021:3(3):1–15. https://doi.org/10.1002/leg3.95

Nkomo GV, Sedibe MM, Mofokeng MA. Phenotyping cowpea accessions at the seedling stage for drought tolerance in controlled environments. *Open Agric*. 2022:7(1):433–444. https://doi.org/10.1515/opag-2022-0093

Ohlsson JA, Leong JX, Elander PH, Ballhaus F, Holla S, Dauphinee AN, Johansson J, Lommel M, Hofmann G, Betner S, *et al*. SPIRO-the automated Petri plate imaging platform designed by biologists, for biologists. *Plant J*. 2024:118(2):584–600. https://doi.org/10.1111/tpj.16587

Petrozza A, Santaniello A, Summerer S, Di Tommaso G, Di Tommaso D, Paparelli E, Piaggesi A, Perata P, Cellini F. Physiological responses to Megafol® treatments in tomato plants under drought stress: a phenomic and molecular approach. *Sci Hortic*. 2014:174(1):185–192. https://doi.org/10.1016/j.scienta.2014.05.023

Polishchuk OV. Stress-related changes in the expression and activity of plant carbonic anhydrases. *Planta*. 2021:253(2):58. https://doi.org/10.1007/s00425-020-03553-5

Rahaman MM, Ahsan MA, Gillani Z, Chen M. Digital biomass accumulation using high-throughput plant phenotype data analysis. *J Integr Bioinform*. 2017:14(3):20170028. https://doi.org/10.1515/jib-2017-0028

Ravelombola W, Shi A, Chen S, Xiong H, Yang Y, Cui Q, Olaoye D, Mou B. Evaluation of cowpea for drought tolerance at seedling stage. *Euphytica*. 2020:216(8):1–19. https://doi.org/10.1007/s10681-020-02660-4

Rossi R, Costafreda-Aumedes S, Leolini L, Leolini C, Bindi M, Moriondo M. Implementation of an algorithm for automated phenotyping through plant 3D-modeling: a practical application on the early detection of water stress. *Comput Electron Agric*. 2022:197:106937. https://doi.org/10.1016/j.compag.2022.106937

Rouphael Y, Colla G. Editorial: biostimulants in agriculture. *Front Plant Sci*. 2020:11:40. https://doi.org/10.3389/fpls.2020.00040

Satoh Y, Yoshimura K, Pokhrel Y, Kim H, Shiogama H, Yokohata T, Hanasaki N, Wada Y, Burek P, Byers E, *et al*. The timing of unprecedented hydrological drought under climate change. *Nat Commun*. 2022:13(1):3287. https://doi.org/10.1038/s41467-022-30729-2

Singh A, Breja P, Khurana JP, Khurana P. Wheat Brassinosteroid-Insensitive1 (TaBRI1) interacts with members of TaSERK gene family and cause early flowering and seed yield enhancement in arabidopsis. *PLoS One*. 2016:11(6):e0153273. https://doi.org/10.1371/journal.pone.0153273

Tardieu F, Cabrera-Bosquet L, Pridmore T, Bennett M. Plant phenomics, from sensors to knowledge. *Curr Biol*. 2017:27(15):R770–R783. https://doi.org/10.1016/j.cub.2017.05.055

Trontin C, Kiani S, Corwin JA, Hématy K, Yansouni J, Kliebenstein DJ, Loudet O. A pair of receptor-like kinases is responsible for natural variation in shoot growth response to mannitol treatment in Arabidopsis thaliana. *Plant J*. 2014:78(1):121–133. https://doi.org/10.1111/tpj.12454

Valle B, Simonneau T, Boulord R, Sourd F, Frisson T, Ryckewaert M, Hamard P, Brichet N, Dauzat M, Christophe A. PYM: a new, affordable, image-based method using a Raspberry Pi to phenotype plant leaf area in a wide diversity of environments. *Plant Methods*. 2017:13:98. https://doi.org/10.1186/s13007-017-0248-5

Verbree DA, Singh BB, Payne WA. Genetics and heritability of shoot drought tolerance in cowpea seedlings. *Crop Sci*. 2015:55(1):146–153. https://doi.org/10.2135/cropsci2014.02.0137

Walter A, Liebisch F, Hund A. Plant phenotyping: from bean weighing to image analysis. *Plant Methods*. 2015:11:14. https://doi.org/10.1186/s13007-015-0056-8

Wang J, Zhang Z. GAPIT version 3: boosting power and accuracy for genomic association and prediction. *Genom Proteom Bioinform*. 2021. https://doi.org/10.1016/j.gpb.2021.08.005

Wang L, Jin X, Li Q, Wang X, Li Z, Wu X. Comparative proteomics reveals that phosphorylation of β carbonic anhydrase 1 might be important for adaptation to drought stress in brassica napus. *Sci Rep*. 2016:6(1):39024. https://doi.org/10.1038/s41598-016-0001-8

Wickham H. ggplot2: elegant graphics for data analysis. New York: Springer-Verlag; 2016. https://ggplot2.tidyverse.org

Xiao Z, Lam H. ShinySyn: a Shiny/R application for the interactive visualization and integration of macro- and micro-synteny data. *Bioinformatics*. 2022:38:4406–4408. https://doi.org/10.1093/bioinformatics/btac503

Yang W, Duan L, Chen G, Xiong L, Liu Q. Plant phenomics and high-throughput phenotyping: accelerating rice functional genomics using multidisciplinary technologies. *Curr Opin Plant Biol*. 2013:16(2):180–187. https://doi.org/10.1016/j.pbi.2013.03.005

Yu L, Julkowska MM. BTI mobile plant phenotyping system: image analysis protocol. *protocol.io*. 2022:1:1–17. https://doi.org/10.17504/protocols.io.8epv59oz4g1b/v1

Yuan H, Liu D. Functional disruption of the pentatricopeptide protein SLG1 affects mitochondrial RNA editing, plant development, and responses to abiotic stresses in Arabidopsis. *Plant J*. 2012:70(3):432–444. https://doi.org/10.1111/j.1365-313X.2011.04883.x

Zhang H, Ge Y, Xie X, Atefi A, Wijewardane NK, Thapa S. High throughput analysis of leaf chlorophyll content in sorghum using RGB, hyperspectral, and fluorescence imaging and sensor fusion. *Plant Methods*. 2022:18(1):60. https://doi.org/10.1186/s13007-022-00892-0

Zhang H, Zhao Y, Zhu J. Thriving under stress: how plants balance growth and the stress response. *Dev Cell*. 2020:55(5):529–543. https://doi.org/10.1016/j.devcel.2020.10.012

Zhang Y, Liu JS. Fast and accurate approximation to significance tests in genome-wide association studies. *J Am Stat Assoc*. 2011:106-(495):846–857. https://doi.org/10.1198/jasa.2011.ap10657

Zhao C, Zhang Y, Du J, Guo X, Wen W, Gu S, Wang J, Fan J. Crop phenomics: current status and perspectives. *Front Plant Sci*. 2019:10:714. https://doi.org/10.3389/fpls.2019.00714

Zhou J, Chen H, Zhou J, Fu X, Ye H, Nguyen HT. Development of an automated phenotyping platform for quantifying soybean dynamic responses to salinity stress in greenhouse environment. *Comput Electron Agric*. 2018:151:319–330. https://doi.org/10.1016/j.compag.2018.06.016

Zhou S, Chai X, Yang Z, Wang H, Yang C, Sun T. Maize—IAS: a maize image analysis software using deep learning for high-throughput plant phenotyping. *Plant Methods*. 2021:17(1):48. https://doi.org/10.1186/s13007-021-00747-0